Adaptive Cruise Control and Driver Modeling

Johan Bengtsson

Department of Automatic Control
Lund Institute of Technology
Lund, November 2001

Department of Automatic Control
Lund Institute of Technology
Box 118
S-221 00 LUND
Sweden

ISSN 0280–5316
ISRN LUTFD2/TFRT--3227--SE

Printed in Sweden,
Lund University, Lund 2001

Contents

Acknowledgments

First of all, I would like to thank my supervisor Rolf Johansson for his guidance and for many stimulating discussions. It is a pleasure to work at the Dept. of automatic Control consisting of talented people, good facilities and a great atmosphere. Therefore, I would like to thank you all. I would specially want thank Bo Lincoln and Anders Robertsson.

At Volvo Technical Development I would like to thank Agneta Sjögren, Eric Hesslow and Fredrik Botling for the assistance and help. I also want to thank Mathias Haage at Dept. Computer science, Lund Institute of Technology whose comments on my work have been valuable.

This work has been supported by Volvo Technical Development and VINNOVA (Swedish Agency for Innovation Systems) formerly called NUTEK (Swedish National board for Industrial and Technical Development).

Johan Bengtsson

1

Introduction

1.1 Background and Motivation

Systems that support a driver in traffic situations and reduce the total driver workload, is a growing research topic. Several of these support systems aim toward full or partial automatic driver assistance, such as those for longitudinal control that are often called Adaptive Cruise Control (ACC) systems. Adaptive cruise control distinguishes itself from cruise control in its use of sensors that measure the headway distance and a controller which adjusts the velocity and distance to the vehicle in front. Adaptive cruise control requires appropriate sensor technology, actuators and control devices and its system design requires data acquisition, control system design and validation procedures. The motivation for these systems is that they aim at increasing the driving comfort, reducing traffic accidents and increasing the traffic flow throughput. The ACC systems autonomously adjust the vehicle's speed according to current driving conditions. In order to accomplish driver comfort the system must resemble driver behavior in traffic. The system must avoid irritation of the driver and of the surrounding traffic. Therefore, to design a system that resembles the natural longitudinal behavior of a driver a good model is needed. There exist several attempts to model the drivers' longitudinal behavior, which all aim at describing various parts of the drivers' behavior. The model structures are different, some are based on cognitive models or general longitudi-

nal models or only car-following models. Most of them have one thing in common in that they are using static models.

The main contributions of the thesis are:

- An experimental platform for adaptive cruise control and driver modeling;
- Contribution to the description of human driver's longitudinal driver behavior using dynamic models;
- The use of system identification methods to obtain the driver models useful for adaptive cruise control.

Experiments in which seven drivers participated have been performed for a variety of different traffic situations. The collected data have been analyzed and used in the estimation of the driver models.

2

Review of driver models

2.1 Introduction

Human driver behavior has been studied since the beginning of the 1950s, but during the 1990s the topic has grown considerably.

The division of driver behavior into separately studied parts has been a common theme of the field, since a general driver model is inherently complex. For example, there exist separate models for describing steering behavior, driver work load, safety behavior and longitudinal behavior.

This chapter concentrates on a review of different longitudinal behavior models. A longitudinal model describes vehicle acceleration behavior using throttle and brakes as input signals.

2.2 Human driver models

The study of the human driver behavior in car-following situations started in the 1950s and has since been an extended topic. The general form of the car-following driver models developed in the 1950s is based on the assumption that each driver reacts in a specific fashion to a stimulus, which leads to an actuation of the acceleration. Stimulus may be a change in the headway distance or a change in the environment condition.

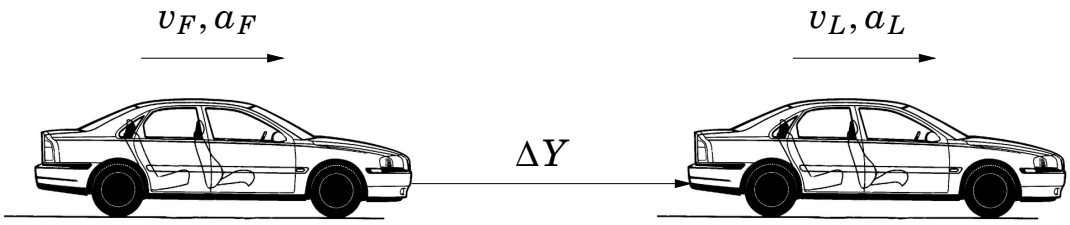

Figure 2.1 Car-following

This leads to a stimulus-response model:

$$r_n(t) = k_n(t - \tau_n) \cdot s_n(t - \tau_n) \tag{2.1}$$

where

$r_n(t) =$ acceleration applied at time t for driver n
$k =$ sensitivity
$s =$ stimulus
$t =$ time of observation
$\tau_n =$ reaction time for driver n (Includes the time for both perception and action)

Car-following models describe the drivers longitudinal behavior in situations such as in Fig. 2.1. In these situations the driver is following another car and tries to maintain a driver specific headway distance to the front car.

A simple human-driver model in car-following tasks can simplified be represented as in Fig. 2.2.

All of the early work in car-following driver modeling assumes that the driver is able to percept the space headway and the relative speed between his car and the lead car. Chandler *et al*. [10] developed a linear car-following model based on this general stimulus-response relationship. Mathematically, the model can be expressed as:

$$a_F(t) = \frac{\lambda}{M}[v_L(t - \tau) - v_F(t - \tau)] \tag{2.2}$$

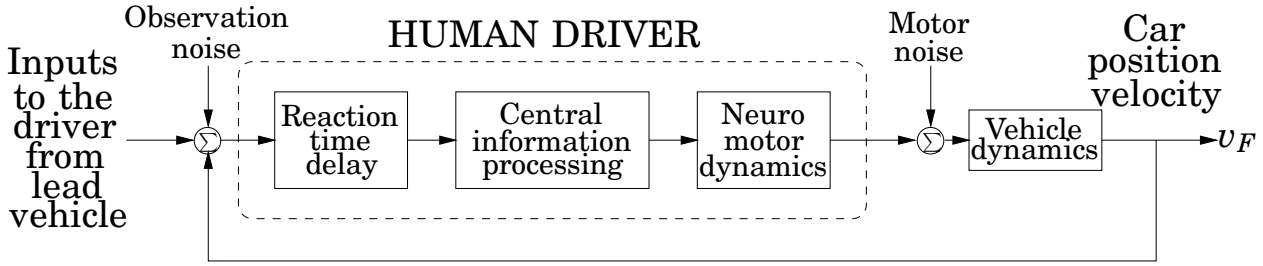

Figure 2.2 Structure of a human driver in car-following

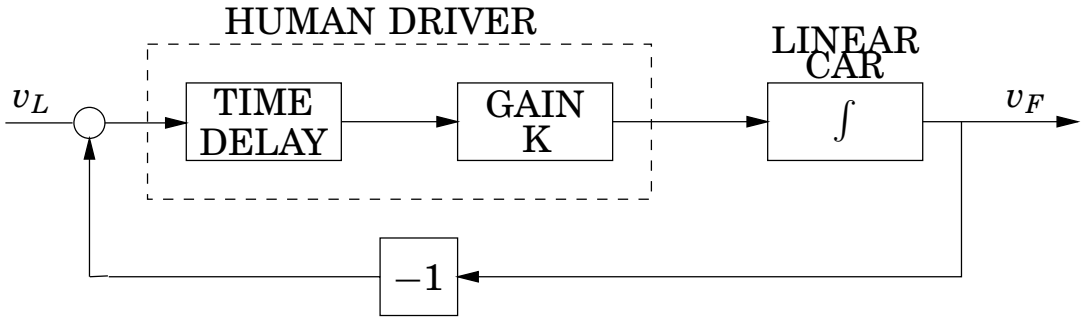

Figure 2.3 Car-following model

where

$$
\begin{aligned}
a_F(t) &= \text{acceleration of the following car} \\
\lambda &= \text{sensitivity factor of the control mechanism} \\
M &= \text{vehicle mass} \\
v_L &= \text{velocity of the leader car} \\
v_F &= \text{velocity of the following car}
\end{aligned}
$$

The model can also be expressed in block diagram, Fig. 2.3.

Chandler *et al*. at the General Motors Technical Center estimated the model using a correlation analysis method and collected car-following data. They used eight male drivers in the study and the experiments showed that the reaction time T was approximately 1.5 seconds and the ratio of sensitivity to mass was approximately 0.37 seconds^{-1}. In this model, the sensitivity term λ or gain was constant for all situations which limits the validity of the model. Gazis *et al*. assumed λ to be dependent on the spacing headway between the cars. In [12] they

developed the following model:

$$a_F(t) = \frac{b}{\Delta Y(t-\tau)}(v_L(t-\tau) - v_F(t-\tau)) \tag{2.3}$$

where

$$b = \text{sensitivity constant}$$
$$\Delta Y(t-\tau) = \text{the space headway at time } (t-\tau)$$

As this model had limitations in low density traffic Edie *et al*. [11] proposed a new model:

$$a_F(t) = b\frac{v_L(t-\tau)}{\Delta Y(t-\tau)^2}(v_L(t-\tau) - v_F(t-\tau)) \tag{2.4}$$

This model performs better than the model proposed by Gazis *et al*. [12] at low traffic densities. Gazis *et al*. [13] developed a model that would be known as the General Motors Nonlinear (GM) model. Mathematically the model can be expressed as:

$$a_F(t) = \alpha\frac{v_L(t)^\beta}{\Delta Y(t-\tau)^\gamma}(v_L(t-\tau) - v_F(t-\tau)) \tag{2.5}$$

where

$$\alpha = \text{constant}$$
$$\beta = \text{model parameter}$$
$$\gamma = \text{model parameter}$$

Gazis *et al*. tried to estimate the model, but they had not sufficient data to claim a certain model to be superior to all others. May and Keller [38] made a rigorous framework to estimate the GM model. In the Gazis *et al* [13] study, β and γ were integers but in the May Keller [38] study the β and γ were allowed to be real values. They found that $\alpha = 1.33\text{e-}4$, $\beta = 0.8$, and $\gamma = 2.8$ gave higher correlation between the observed and estimated accelerations.

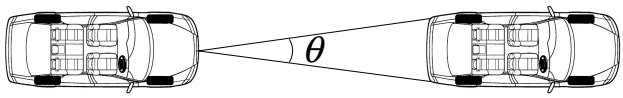

Figure 2.4 The visual angle in car-following

Pipes [42] developed an alternative approach, which is based on the assumption that a driver is using the visual angle enclosing the lead car (Fig 2.4).

The angle θ increases when the following car is approaching the lead car. Using this approach, Pipe developed a model where the acceleration of the following car is proportional to the driver's perception of the rate of change of the visual angle θ. Expressed mathematically:

$$a_F(t) = b\frac{(v_L(t-\tau) - v_F(t-\tau))}{(\Delta Y(t-\tau))^2} \tag{2.6}$$

Addison and Low [1] developed a model based on the assumption that the driver aims at a desired headway and strives to minimize the relative speed Δv. The model is an extension of the Gazis *et al.* [13] including a nonlinear headway-dependent term. Mathematically, the model can be expressed as:

$$a_n(t) = \alpha\frac{v_f(t)^\beta \Delta v(t-\tau)}{(\Delta Y(t-\tau))^\gamma} + \eta(\Delta Y(t-\tau) - D_n)^3 \tag{2.7}$$

where

$$D_n = \text{the desired headway}$$
$$\eta = \text{constant}$$

Linear Optimal Control Model Structure

The optimal control model structure is based on a performance criterion such as that of linear quadratic Gaussian control [3]. Minimization of the performance criteria gives the structure of the controller. This structure differs from the stimulus-response structure, since nonlinearities in the vehicle are included in the model. Bekey [4], who made a review on this model structure, mentioned that even though it may not be reasonable to assume that a human driver should mimic an optimal controller, the result is interesting.

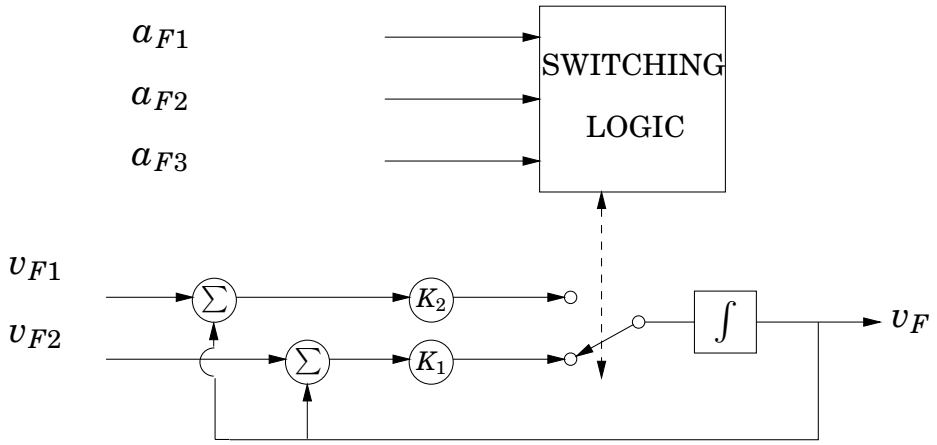

Figure 2.5 Look-ahead model

Rational function model

Bleile [6] proposed a new longitudinal driver model. Bleile used kernel density estimation and found that the most relevant triple of input variables are v_n, ΔY and $v_{n-1} - v_n$ to describe the driver's longitudinal behavior. Choosing a rational function as approach for the relation between the input variables v_n, ΔY and $v_{n-1} - v_n$ and the mean acceleration a_n the model can be expressed as:

$$a_n = f(v_n, \Delta Y, v_{n-1}) + r(v_n, \Delta Y, v_{n-1})\xi(t) \tag{2.8}$$

where

$$f(v_n, \Delta Y, v_{n-1}) = \frac{1 + b_1 v_n + b_2 \Delta Y + b_3 v_n \Delta Y + b_4 v_{n-1} + b_5 v_n v_{n-1}}{c_0 + c_1 v_n + c_2 \Delta Y + c_3 v_n \Delta Y + c_4 v_{n-1} + c_6 \Delta Y v_{n-1}}$$

$$\xi(t) = \text{zero mean white Gaussian noise with a identity power spectral density}$$

Bleile implemented the model as an Extended Kalman Filter with v_{n-1} as input and $\Delta Y, v_n$ as observed variables.

Heuristic human driver models

Bekey [4] also reviewed two heuristic human driver models. The first of these, the look-ahead model (Fig. 2.5), was based on the assumption

that the driver observes the behavior of three cars ahead of him, and that he adjust his own strategy from their behavior. The second model, a finite-state model, is based on the assumption that a human driver always tries to maintain a velocity equal to the lead car along a safe headway.

Adaptive Cruise Control

Ioannou [25] presented an ACC system, which he compared to three human driver models: Linear car-follow model, Linear Optimal Control Model, and Look-ahead Model. Mathematically, the vehicle model can be expressed as:

$$\begin{aligned}
\frac{d}{dt}y_n(t) &= v_n(t) \\
\frac{d}{dt}\dot{y}_n(t) &= a_n(t) \\
\frac{d}{dt}\ddot{y}_n(t) &= b(\dot{y}_n, \ddot{y}_n) + \alpha(\dot{y}_n)u_n(t)
\end{aligned}$$

where

$$\begin{aligned}
\alpha(\dot{y}_n) &= \frac{1}{m_n \tau_n(\dot{y}_n)} \\
b(\dot{y}_n, \ddot{y}_n) &= -2\frac{k_{d_n}}{m_n}\dot{y}_n\ddot{y}_n - \frac{1}{\tau_n(\dot{y}_n)}[\ddot{y}_n + \frac{k_{d_n}}{m_n}\dot{y}_n^2 + \frac{d_{m_n}(\dot{y}_n)}{m_n}] \\
y_n &= \text{position of the } n\text{th vehicle} \\
v_n &= \text{velocity of the } n\text{th vehicle} \\
a_n &= \text{acceleration of the } n\text{th vehicle} \\
m_n &= \text{mass of the } n\text{th vehicle} \\
\tau_n &= n\text{th vehicle's engine time constant} \\
u_n &= n\text{th vehicle's engine input} \\
k_{d_n} &= n\text{th aerodynamic drag coefficient} \\
d_{m_n} &= \text{mechanical drag of the } n\text{th vehicle}
\end{aligned}$$

Control law:

$$u_n = \frac{1}{\alpha(\dot{y}_n)}[c_n(t) - b(\dot{y}_n, \ddot{y}_n)] \tag{2.9}$$

where

$$
\begin{aligned}
c_n &= C_p\delta_n(t) + C_u\dot{\delta}_n(t) + K_v v_n(t) + K_a a_n(t) \\
\delta_n(t) &= y_{n-1}(t) - y_n - (L_n + S_{o_n} + \lambda_2 v_n(t)) \\
\dot{\delta}_n(t) &= v_{n-1}(t) - v_n - \lambda_2 a_n(t) \\
L_n &= \text{length of the } n_{th} \text{ vehicle} \\
S_{o_n} &= \text{initial headway} \\
\delta_n(t) &= \text{deviation from desired headway} \\
C_p &= \text{design constant} \\
C_v &= \text{design constant} \\
K_v &= \text{design constant} \\
K_a &= \text{design constant}
\end{aligned}
$$

Ioannou's conclusion was that the comparison indicates a strong potential for ACC to smoothen traffic flows and to increase traffic flow rates considerably if designed and implemented properly. In this study several emergency situations were simulated and used to demonstrate that the ACC proposed may lead to much safer driving. This ACC model is the foundation for the ACC system now used by Ford.

Neural network and fuzzy logic model.

Ghazi Zadeh *et al*. [15] made a literature survey on this area. The driver models presented in the review all handle lateral guidance and some of them also include longitudinal guidance. Several of the driver models in the survey are for autonomous vehicle following, e.g., Griswold [19]. Germann and Isermann [14] proposed an intelligent cruise control (ICC) based on fuzzy logic and neural networks. They use a three-layer structure, Fig. 2.6.

In the first layer, a linearization of the nonlinearities is made. The second layer consists of a linear acceleration controller, based on classical controlling techniques and the third layer consist of a fuzzy controller, based on the linguistic description of comfort demands.

The fuzzy controller (Fig 2.7) is based on the different 'linguistic' input variables: distance, velocity, relative velocity, and actual velocity.

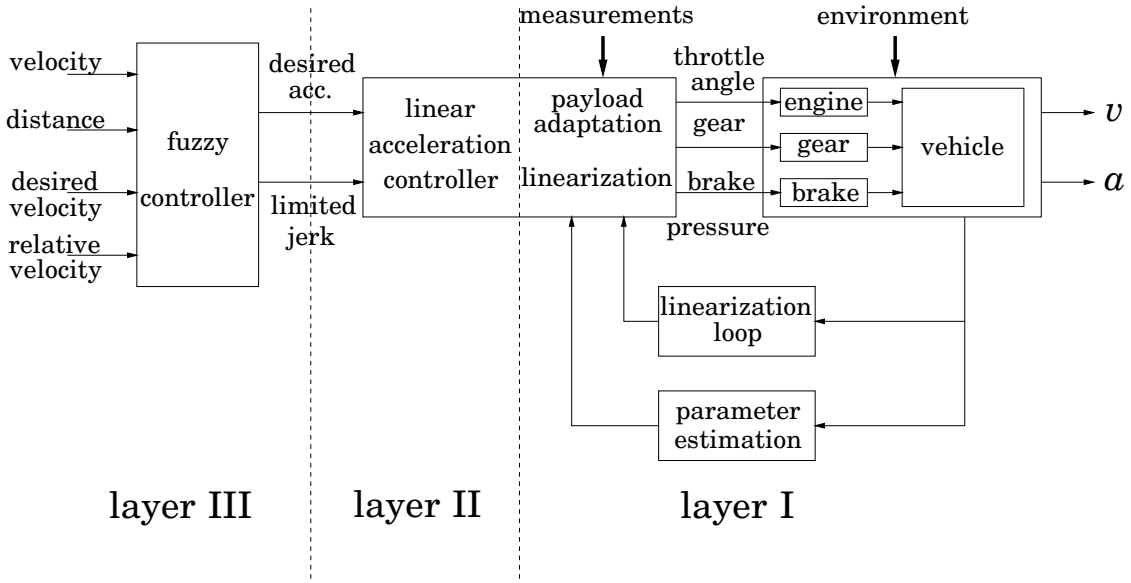

Figure 2.6 Controller structure for fuzzy cruise control.

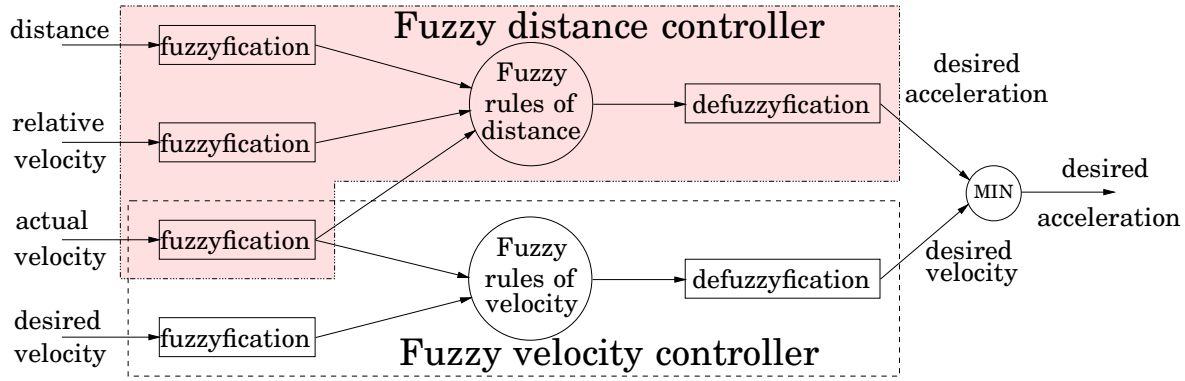

Figure 2.7 Fuzzy-logic controller

The output acceleration is obtained by:

$$a = \min[a(\text{velocity}), a(\text{distance})] \tag{2.10}$$

Additionally they replace the two fuzzy controllers by an artificial neural network, which they trained by measurement data. The ICC is implemented, and tested both in highway traffic and in stop-and-go traffic on highway congestion.

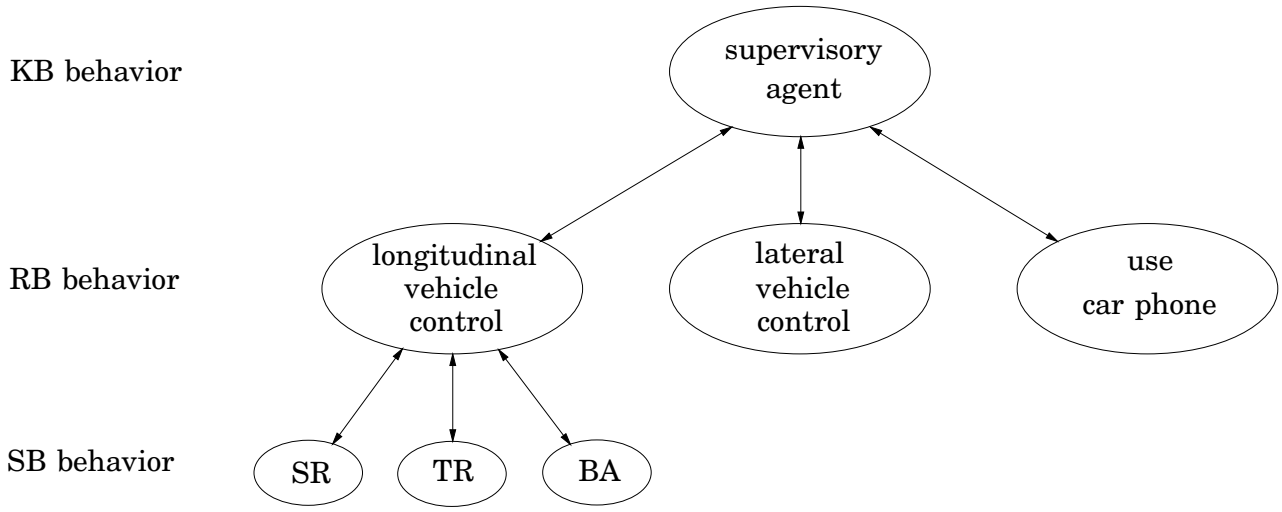

Figure 2.8 Hierarchical structure of the mental model [17]

Mental models

Goodrich and Boer [17] proposed a mental model to describe the human driver behavior. A mental model is an internal representation employed to encode, predict, evaluate, and communicate the consequences of perceived and intended changes to the operator's current state within the dynamic environment [30]. To describe the human driving behavior multiple mental models are used, which can be organized into a society of interacting agents (Fig. 2.8). The mental models are organized in a three level hierarchical structure, which corresponds to Rasmussen's knowledge-based (KB), rule-based (RB), and skill-based (SB) behaviors [44]. The model include, at the RB level, car phone usage, in order to see how attention is shared between agents.

Although Goodrich and Boer did not provide a complete formulation of the proposed model, they provided a preliminary computational model to emulate RB and SB behaviors. Boer *et al.* [7] have also proposed an integrated driver model, which incorporate the dynamical aspects of driver behavior and the role of driver needs (Fig. 2.9).

Using this structure, Kuge *et al.* [34] proposed a driver behavior recognition model based on the Hidden Markov Model (HMM). They developed a HMM driver behavior model recognition in lane changes, which they validate. A favorable property of this method is that it detects a lane change very early in the stage of steering. In order to

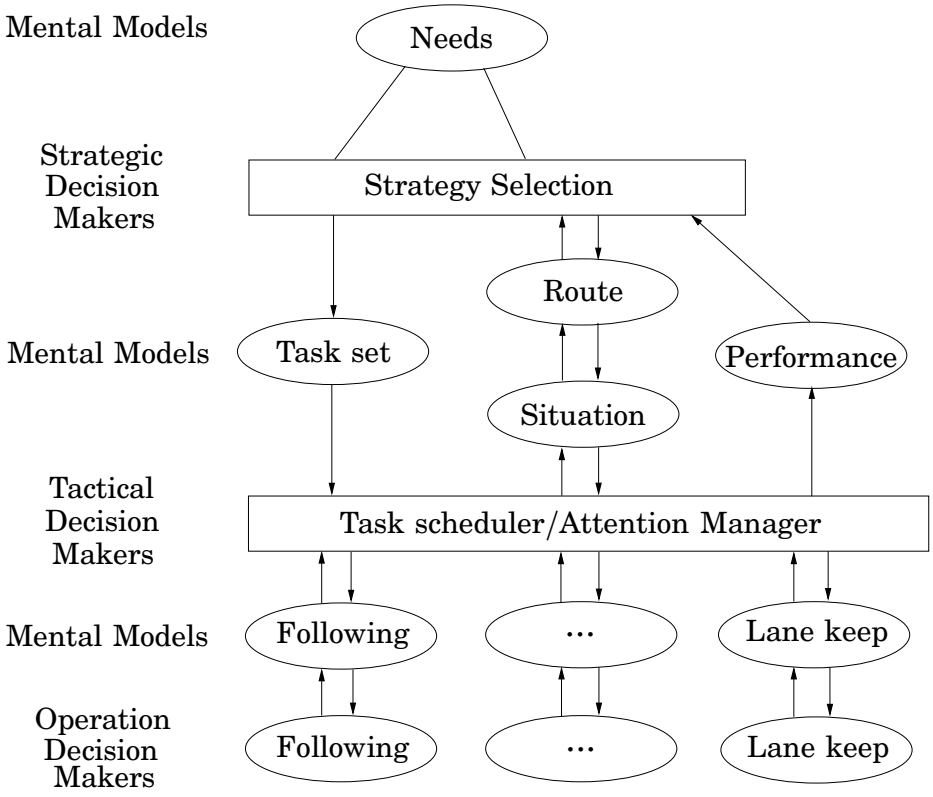

Figure 2.9 Integrated driver model [7]

base driver assistance on HMM driver behavior recognition, more work will have to be done. General models of lane changing recognition will have to be developed and robustness will have to be assured. Kiencke and Nielsen [33] presented a hybrid driver model aiming to describe the complete cognitive process of the human operator.

2.3 General longitudinal driver behavior

Leutzbach [36] proposed a psycho-physical spacing model where he introduced the term "perceptual threshold" to define the behavior of the driver. If the stimulus is smaller than the threshold then the driver is influenced of the lead car and if the stimulus exceeds the threshold the driver is uninfluenced of the lead car. Even if Leutzbach did not provide any mathematical suggestion how this threshold could be estimated, it was a first step to more general models of the driver's longitudinal be-

havior. Wiedermann [53] extended the Leutzbach model and presented how to calculate the thresholds and how to perform simulation. Wiedermann wanted to cover the whole range of drivers' behavior, poor as well as good. Therefore, the single parameters of the model are normally distributed and standardized around a median. The driver model distinguishes between four driving situations, in which drivers behave in significantly different ways. Wiedermann introduced the individual driving parameters: desired speed, want for safety and reaction time in different driving situations. He used these to determine the drivers' levels of perception. The four driving situations are:

- **Uninfluenced driving:**
  In this driving situation the driver is uninfluenced of other cars, and he/she attain his/her desired speed. The driver's desired speed is reasonably constant, determined by a compromise between desire for safety on the one hand and minimizing the trip duration on the other hand.

- **Approaching:**
  Consciously influenced driving. The driver is closing up the front car. The driver has reached his/her individual reaction distance, ΔY_r, and begins to slow down. During this situation, the driver decreases his/her speed and aims to adjust his/her speed to the speed of the vehicle in front. The headway distance aimed at by the driver during the approach is individual and is essentially depending on the driver's desire of safety.

- **Braking:**
  Consciously influenced driving. The headway distance sinks under the driver individual minimal headway distance, ΔY_{min}. The driver brakes to reestablish the minimal headway distance. When the driver has established his/her individual headway the driver changes either from approaching or from braking into car-following.

- **Car-following:**
  Unconsciously influenced driving. Follows the leading vehicle and tries to maintain his/her desired headway and will vary with the distance from the desired headway. The variation will be between

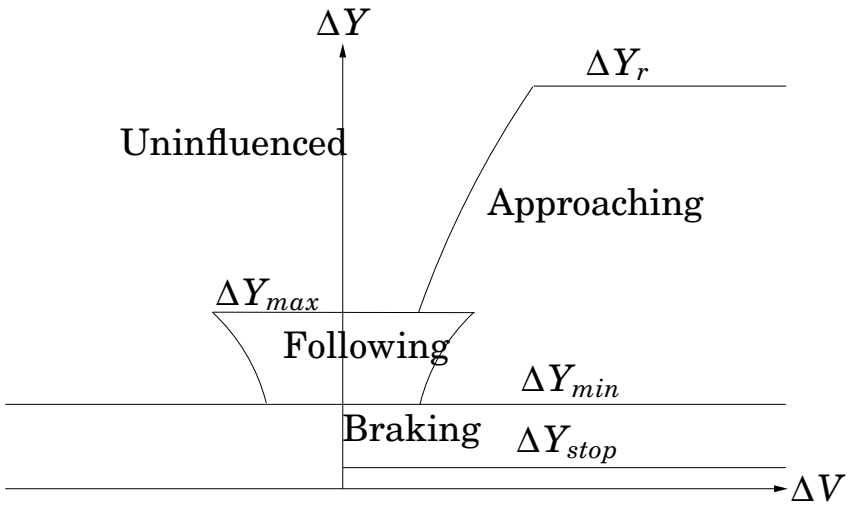

Figure 2.10 Driving situations and the different levels of perception

an individual maximal following distance and an individual minimal following distance. If the headway distance is not in that interval, the driver will switch from car-following to one of the other three driving situations.

$$\begin{aligned}
\Delta Y_{\text{stop}} &= 5.5 + Z_{F1} \\
\Delta Y_{\text{min}} &= \Delta Y_{\text{stop}} + (1 + 7 \cdot Z_{F1}) \cdot \sqrt{(V_F)} \\
\Delta Y_{\text{max}} &= \Delta Y_{\text{stop}} + (2 - Z_{F2} + N_{ZF}) \cdot (\Delta Y_{\text{min}} - \Delta Y_{\text{stop}}) \\
\Delta Y_r &= ((\Delta Y - \Delta Y_{\text{stop}})/(25 \cdot (1 + Z_{F1} + Z_{F2})))^2
\end{aligned}$$

With Z_{F1} = driver's need for safety [0..1], Z_{F2}= driver's perception ability, N_{ZF} = driver's situation dependent model parameter.

Recently, Institut für Kraftfahrwesen Aachen (IKA) and BMW created the microscopic traffic simulation program PELOPS (Program for the dEvelopment of Longitudinal micrOscopic traffic Process in a System relevant environment), developed 1990-1994, using Wiedermann's model [37].

Gipps [16] presented a general car-following model that also works in the uninfluenced regime. The model is based on the assumption that the driver sets limits to his/her desired braking and acceleration rates and using these limits to calculate the desired speed. He also used the

assumption that the driver selects a speed where he is ensured that he can perform a safe stop if the lead car is doing a sudden stop. Gipps calculated the maximum acceleration for the driver such that it will not exceed the driver's desired speed. He did not estimate the individual reaction time, but instead used constant reaction time of 2/3 seconds for all drivers. The parameters in the model were estimated, but not in a rigorous framework.

Benekohal and Treiterer [5] developed an acceleration algorithm where they separated the acceleration and deceleration rates in the following five situations:

1. The following car is moving but has not reached the desired speed.
2. The following car has reached the desired speed.
3. The following car was stopped and has to start from a stand-still position.
4. The car-following algorithm governs the following car's performance while space headway constraint is satisfied.
5. The car is advanced according to the car-following algorithm with non-collision constraint.

No rigorous framework for parameter estimation was presented. Using this acceleration model they developed a car-following model, called CARSIM, which simulated traffic both in normal and in stop-and-go conditions. Yang and Koutsopoulus [55] developed a general longitudinal driver model depending on the headway as classified driver into the following regimes: uninfluenced driving, car-following, and emergency deceleration. In the emergency regime the driver use an appropriate deceleration to avoid collision. In the car-following regime they used the known GM model. Ahmed [2] developed a model build on earlier work by Subramanian [45] and extended it. Ahmed's model has two regimes uninfluenced regime and car-following regime. The sensitivity factors in the car-following during acceleration and deceleration differs. The model includes the traffic density ahead of the car. Ahmed's model is mathematically expressed as:

$$a_n(t) = \begin{cases} a_n^{cf}(t), & if\, h_n(t-\tau_n) \leq h_n^* \\ a_n^u(t), & o.w. \end{cases} \tag{2.11}$$

where

$$\begin{aligned}
\tau_n &= \text{reaction time for driver } n \\
a_n^{cf} &= \text{car following acceleration} \\
a_n^{u} &= \text{uninfluenced acceleration} \\
h_n(t-\tau_n) &= \Delta Y_n(t-\tau_n)/v_n(t-\tau_n), \text{ the time headway} \\
h_n^{*} &= \text{unobserved headway threshold for driver } n
\end{aligned}$$

The car-following model

$$a_n^{cf}(t) = s[Y_n^{cf,g}(t-\xi\tau_n)]f[\Delta v_n(t-\tau_n)] + \varepsilon_n^{cf,g}(t) \tag{2.12}$$

where

$$\begin{aligned}
g &\in [\text{acc}, \text{dec}] \\
s[Y_n^{cf,g}(t-\xi\tau_n)] &= \text{sensitivity} \\
\xi &\in [0,1], \text{a parameter for sensitivity lag} \\
f[\Delta v_n(t-\tau_n)] &= \text{stimulus} \\
\varepsilon_n^{cf,g}(t) &= \text{random term associated with the car-following} \\
&\quad \text{acceleration of driver } n \text{ at time } t
\end{aligned}$$

The stimulus is a function of the relative speed, Fig. 2.11. When ΔV is low drivers is not able to percept a small deviation of the relative speed, but for ΔY larger than a certain threshold, $|\Delta V_1|$, drivers get a better sense of the stimulus and therefore, increase the acceleration at an increasing rate. When the ΔV gets larger than the threshold $|\Delta V_2|$, the acceleration applied by the driver is limited by the acceleration capacity of the vehicle.

The model sensitivity and stimulus function is:

$$s[Y_n^{cf,g}(t-\xi\tau_n)] = \alpha^g \frac{V_n(t-\xi\tau_n)^{\beta^g}}{\Delta Y(t-\xi\tau_n)^{\gamma^g}} k_n(t-\xi\tau_n) \tag{2.13}$$

$$f[\Delta v_n(t-\tau_n)] = \Delta V_1((t-\tau_n)^{\lambda_1^g} + \Delta V_2(t-\tau_n)^{\lambda_2^g} + \Delta V_3(t-\tau_n)^{\lambda_3^g} \tag{2.14}$$

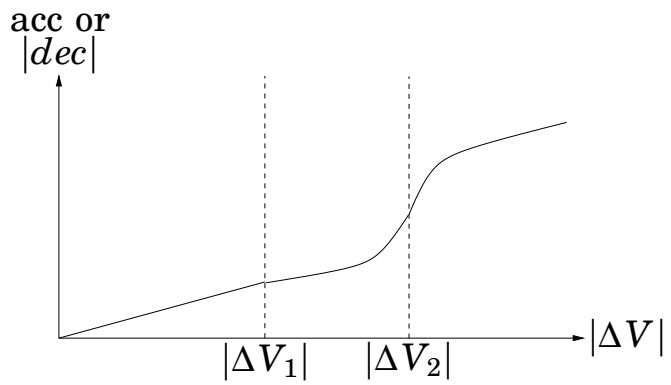

Figure 2.11 Impact of the relative speed on drivers' acceleration decision

where

$$\begin{aligned}
\Delta V_1(t-\tau_n) &= \min(|\Delta V_n(t-\tau_n)|, |\Delta V 1|) \\
\Delta V_2(t-\tau_n) &= \max(|\Delta V_n(t-\tau_n)| - |\Delta V_1|, |\Delta V_2| - |\Delta V_1|) \\
\Delta V_3(t-\tau_n) &= \max(0, |\Delta V_n(t-\tau_n)| - |\Delta V_2|) \\
k(t-\xi\tau_n) &= \text{density of traffic ahead of the car within its view}
\end{aligned}$$

$$a_n^u(t) = \lambda^u[V_n^*(t-\tau_n) - V_n(t-\tau_n)] + \varepsilon_n^u(t) \tag{2.15}$$

where

$$\begin{aligned}
\lambda^u &= \text{sensitivity} \\
V_n^*(t-\tau_n) &= \text{desired speed of the driver} \\
V_n^*(t-\tau_n) - V_n(t-\tau_n)] &= \text{stimulus} \\
\varepsilon_n^u(t) &= \text{random term associated with the unifluenced acceleration of driver } n \text{ at time } t
\end{aligned}$$

The headway threshold, h^*, is assumed to be normally distributed truncated beyond $h^*_{\min}, h^*_{\max}$.

$$f(h_n^*) = \begin{cases} \dfrac{\frac{1}{\sigma_h}\phi(h_n^* - \mu_h)}{\Phi(\frac{h^*_{\max} - \mu_h}{\sigma_h}) - \Phi(\frac{h^*_{\min} - \mu_h}{\sigma_h})} & h^*_{\min} \le h_n^* \le h^*_{\max} \\ 0, & \text{otherwise} \end{cases} \tag{2.16}$$

where

$$\begin{aligned} \mu, \sigma &= \text{mean and standard deviation of the untruncated distribution} \\ h^*_{\min}, h^*_{\max} &= \text{minimum and maximum values of } h^*_n \\ \phi &= \text{probability density function} \\ \Phi &= \text{distribution function} \end{aligned}$$

2.4 The human driver brake behavior

Lee [35] proposed that the driver use the simplest type of visual information from the optic flow, which is sufficient for controlling braking. That is time-to-collision information (TTC) , not information about distance, relative speed, or acceleration. The driver bases his judgment on TTC information, when to start braking and to control the braking action. Van Der Horst [48] supported this assumption, and performed a framework which shows that both the decision when to start braking and how to control the braking progress are based on TTC information available from the optic field. In the study, it is also noticeable that a driver often brakes with a rather constant deceleration during the brake procedure. Van Winsum and Heino [49] proposed the following hypotheses:

- Preferred time-headway is constant over different speeds;
- Preferred time-headway is consistent within individual drivers, but differs between drivers;
- The initiation of braking, measured by brake reaction time (BRT), is more strongly related to TTC at the moment the lead vehicle starts to brake for short followers compared to long followers. This is assumed to be related to differences in the ability to perceive TTC information;
- Preferred time-headway is related to the intensity of braking and quality of braking control. The maximum percentage brake pressed measures the intensity of braking while the quality of

braking control is measured by the sensitivity of the braking intensity to criticality and by the time difference between $t_{\mathrm{TTC}_{\mathrm{min}}}$ and $t_{\mathrm{DEC}_{\mathrm{max}}}$.

Usually BRT was measured as the time from the presentation of the stimulus until the foot touches the brake pedal, $t_{\mathrm{TTC}_{\mathrm{min}}}$ being the time when the minimum TTC is reached during braking, and $t_{\mathrm{DEC}_{\mathrm{max}}}$ being the time when the maximum deceleration is reached during braking.

Winsum and Heino performed experiments to validate the hypothesis, and based on the experiments they concluded that preferred time-headway is constant over different speeds and it is consistent within individual drivers [49]. But there was no evidence that short followers and long followers differ in sensitivity of BRT and the moment the lead vehicle starts to brake. According to the last hypothesis, preferred time-headway is related to the intensity of braking and quality of braking control, not either confirmed, but it was found that the intensity of braking is partly programmed and based on TTC.
Johansson and Rumer [27] estimated the driver brake reaction time using data collected from 321 drivers in real traffic. By using sound as stimulus for braking and measuring the time until the brake light turned on, they found that the brake reaction time varied from 0.4 to 2.7 seconds, with a mean, and standard deviation of 1.01, and 0.37 seconds. Since the drivers were informed that they were participating in a brake reaction study and the use of sound as stimulus, these values may be biased.

2.5 Safety

Often is it suggested that ACC will increase the safety in traffic. The motivation for this is that the ACC give the driver assistance in the driving tasks. The assistance will it reduce the driver's workload, which allows the driver to concentrate more on other tasks. This implies that the drivers will experience less fatigue of driving and that the driving will become more comfortable. The purpose of the ACC is to provide support to the driver in a wide range of driving environments, but the full responsibility will always be on the driver. One objection to

that ACC increase the safety is that the driver may be over-reliant on the ACC system and may not be prepared to take control of the vehicle in extreme situations. Hitz *et al*. [23] have done a field operational test in order to evaluate the safety of ACC in traffic. This test involved 108 drivers, which were studied for a year. In this safety study they use a list of standard surrogate measures of safety. They also extended this to include new safety surrogates and performance measures. Hitz *et al*. compared ACC driving with manual driving and conventional cruise control (CCC) driving. In this study it was found that the ACC drivers tended to wait for the system to control situations and therefore intervened later when necessary which led to that brake pressure above -0.1g where more commonly among ACC drivers, but this did not in general result in extreme situations. It also shows that the drivers using ACC had a longer response time than human drivers and slightly less than CCC drivers did. Since the ACC drivers have greater headway distance than manual drivers do, it is not clear that the longer response time implies inattentiveness by the driver. In the study the drivers ranked the manual driving as most safe followed by ACC driving and CCC driving last. But they also agreed that ACC would improve safety. Hitz *et al*. made a Monte Carlo computer simulation using the data from the test study in order to estimate the safety effects of wide spread ACC use [23]. Their simulation showed that two types of collisions on freeways would be reduced by 17 percent:

- Situations when an ACC equipped vehicle approaching a slower vehicle traveling at constant velocity.

- Situations when the lead vehicle decelerating in front of an ACC equipped vehicle.

The Hitz's *et al*. conclusion of this field test was that if the ACC system would be widespread and fully implemented it would result in a net increase of safety. They did not propose what should be the highest value of deceleration in an ACC system. This would require more study. Today this deceleration authority differs among the systems available. Iijima *et al*. [24] found that 90 percent of all decelerations is less than $2.5 m/s^2$. In BMW's ACC system by Prestl *et al*. [43], a highest deceleration of $-2 m/s^2$ was used. Prestl *et al*. found this to be a suitable

compromise between customer benefit, convenience and safety. This low limit will ensure that the system limits are reached frequently and will not lead the driver to become over-reliant on the system. Prestl *et al*. also shared Hitz *et al*. opinion that a new driver must learn how to use an ACC system properly and understand its limits.

Prestl *et al*. have chosen not to have an audible take-over alarm, the reason is that this could be misunderstood as a collision warning. During their work, they found that a driver is very sensitive to kinesthetic feedback in the beginning of a deceleration, which will raise the driver attention. Therefore experienced drivers do not need any take-over alarm and they also have learned when to start braking. Neither Hitz *et al*. or Prestl *et al*. presented any idea how to best teach a new driver these new requirements placed on him. Prestl *et al*. also presented a technical safety concept, which includes safety in distributed system and shutdown mechanism.

All ACC systems aim towards reducing the driver's workload, which will lead to increased comfort. Nakayama *et al*. [40] proposed a method of measuring the driver workload, called "The steering entropy method". By measuring the driver's variation in the steering angle during driving, it was possible to evaluate the workload. Iijima *et al*. [24] used this method to conclude that their suggested ACC driving reduced the workload in compare with CCC driving. In this study both experienced drivers and novice drivers participated.

2.6 Existing systems

With Navlab at Carnegie Mellon University, Thorpe et. al [47] developed a Free Agent system, which fully automates driving. Their strategy was to surround the vehicles with sensors, putting all the sensing and decision-making in the vehicles to make them fully automated. The automated vehicles were equipped with a vision system, and a radar system. Since the most important mission for the automated vehicle was to increase the safety on the highways, the Free Agent was designed to keep a safe space around the vehicle. The Free Agent aims to have a large enough headway between vehicles that high-bandwidth

throttle and brake servo are not needed. Since only low-bandwidth control is needed, the existing cruise control could be used to perform all the throttle actuation. The Free Agent was demonstrated in August 1997 for the UN National Automated Highway System Consortium. During the demo several of the common actions at highways were performed, but not any cut-in or critical situations.

As of November 2001, BMW started introducing its new ACC system, which will be available in the 7-series. This new ACC system was described by Prestl *et al*. [43] as a complete system including technology and properties of the radar to a human machine interface. They also studied the safety aspects of ACC. BMW's intentions with the ACC system is to enhance the driver's comfort and to support the driver in follow situations. The system was developed in close cooperation with Robert Bosch GmbH, which designed and built the ACC sensor. This module also use information about the current gear, which is provided by BMW's Transmission Control Unit. The presented ACC system is divided into four basic parts, (Figure 2.12):

- Situation specific control functions: Set Speed Controller, Follow Controller and Curve controller;
- Combination and selection respectively as well as limitation of the specific control values in the Mixer;
- Conversion of the acceleration value into desired values for the actuator systems in the Longitudinal Controller;
- Actuator systems that realize controller output.

As other system, for example [24], the FOC aiming to adjust the headway distance to the desired distance and the relative velocity with the preceding vehicle approaching zero.

The following cars are available at the moment:

- Mercedes S-class using radar;
- Jaguar XK series using radar;
- BMW Z9 Convertible concept car using radar;

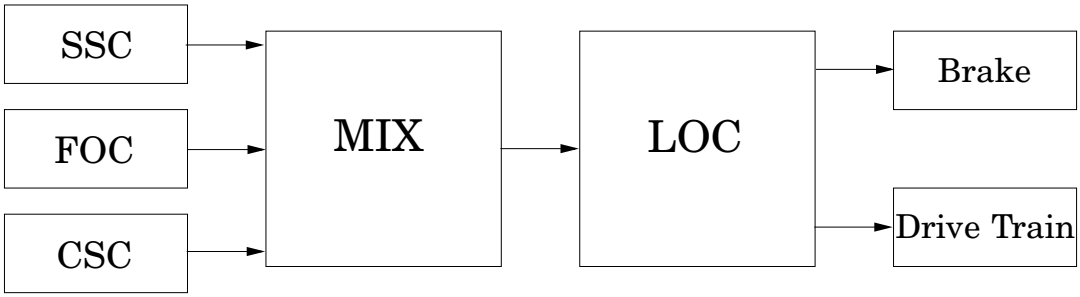

Figure 2.12 BMW's ACC system structure

- Toyota Celsior using laser;
- Toyota Progress using laser;
- Mitsubishi Diamante using laser;
- Lexus LS430 using laser.

2.7 Cut in Situations

In design of an ACC system aiming to increase the driver's comfort, it is necessary understand drivers cut-in behavior. Iijma *et al*. [24] have studied the behavior and included this in theirs ACC model.

2.8 Activities and WWW-links

Automated highway systems at Carnegie Mellon.
`http://www.cs.cmu.edu/XSGroups/ahs/`
Cambridge Basic Research at laboratory of Nissan Technical Center North America, Inc.
`http://pathfinder.cbr.com/`
The Center for Advanced Transportation Technology (CATT) at the University of Southern California.
`http://www.usc.edu/dept/ee/catt/`
Vehicle Dynamics Lab (VDL)at University of California, Berkeley.
`http://vehicle.me.berkeley.edu/`

PATH project
http://www.path.berkley.edu/
The Man Vehicle Laboratory (MVL) at the Massachusetts Institute of Technology.
http://mvl.mit.edu/
The Center for Transportation Analysis (CTA) in the Oak Ridge.
http://www-cta.ornl.gov/cta/research/trb/tft.html
Intelligent Transportation Systems (ITS) at the Massachusetts Institute of Technology.
http://its.mit.edu/

3

Material & Methods

3.1 Introduction

In order to design an ACC which with the drivers feel safe and comfortable, the ACC needs to mimic the driver behavior in traffic. The human driver behavior changes in different traffic situations. Therefore, standard traffic situations have to be identified and used in the experimental phase. Several different drivers are used to capture a range of driver behaviors.

There is a difference between carrying out experiments on public roads and on test tracks. It is assumed that a driver's natural behavior is best caught on public roads. If test tracks are used the subject might show different driver behavior. A possible reason being that the driver feels safer on the test track and as a result drives more aggressively.

Sensors are needed to detect other vehicles in order to study human driver behavior in real traffic situations. Usually the velocity and distance to the vehicle in front are measured.

For this purpose there exist three standard sensors: the radar, the laser, and the camera. The radar is expensive, but is robust to bad weather conditions, like rain, mud, dust or snow. It offers a narrow field-of-view of 8–12 degrees but has a long working range of around 150 meters.

The laser is less expensive, but performs poorly in bad weather because the laser beam is easily blocked by atmospheric particles. The

field-of-view is easily adjustable up to 180 degrees. A typical working range is around 50 meters.

The camera is often used in conjunction with the radar or the laser. It is capable of easily distinguishing between moving and stationary objects. The field-of-view is usually large, depending on the choice of lens.

Sensor field-of-view and range parameter choices are important. For instance, a large field-of-view is advantageous when detecting cut-in vehicles, like cars switching lanes. Small field-of-view sensors, like the radar, does not detect a vehicle until it is almost in front of the driver's vehicle, while a large field-of-view sensor, like the laser or a camera, detects the cut-in vehicle when it starts to switch lanes. The choice of appropriate range depends somewhat on the design philosophy behind the ACC. One opinion is that the sensor should not be better than a human being in order to not introduce a false sense of safety. Other states that the sensor should be as good as possible to enhance the capabilities of the driver driving the vehicle.

Combinations of sensors are used to achieve robust information extraction. The combination of radar and camera uses the camera to compensate for the small field-of-view of the radar and segment moving objects from stationary. This may be a problem when using only range-based sensors like the radar or the laser. The laser and the camera are used in a similar manner. The combination of radar and laser can be used to increase reliability and system robustness. The sensors have different fields-of-view and working range and seldom lose track of the front vehicle at the same time. From a traffic safety point of view this is preferable. Widmann *et. al.* have made a comparison of laser-based and radar-based sensor in ACC [52].

3.2 Experimental platform

Vehicle

Two automatic transmission Volvo 850:s were used in a leading-vehicle-following-vehicle experimental setup (Fig. 3.1). Both vehicles have been used in previous ACC-projects at Volvo Technical Development.

Figure 3.1 One of the two Volvo 850 used in the experiments.

Autoliv-CelsiusTech Electronics	
Modulation characteristics	Modulation type FMCW
Radar scanning principle	Mechanical scanning
Frequency	76-77 GHz
Transmitted power	10mW
Minimum tracking distance	2 m
Maximum tracking distance	200 m
Update rate of radar	10 Hz
Field of view	24°
Angle resolution	0.1°
Distance resolution	1 m

Table 3.1 Radar specification.

They were equipped with a prototype system allowing control of the vehicle's hydraulic brake and throttle angle using control signals from a PC. The following vehicle was equipped with two types of range sensors, radar and laser.

Sensor equipment

A radar from Autoliv-CelsiusTech Electronics was used to measure the distance to the front vehicle ΔY and its relative speed Δv, Table 3.1.

IBEO Laser scanner LD Automotive	
Minimum tracking distance	0.4 m
Maximum tracking distance	100 m
Update rate of laser	10 Hz
Field of view	up to 270°
Angle resolution	0.25°
Distance resolution	0.004 m

Table 3.2 Laser specification

A practical difficulty was that the radar must have good resolution, also at small distances and that the relative speed should be measured with high resolution.

A laser from IBEO, Laser scanner LD Automotive, Fig 3.2, was used to measure ΔY and Δv, Table 3.2.

The reason to use both radar and laser is their complementary working ranges and for redundancy. The radar has a narrow but long working range and the laser has a wide but short working range (Fig. 3.2).

Our earlier work on ACC

Some work on ACC was reported in [41]. In this study a stop-and-go controller for ACC was designed and implemented.

Data acquisition

Drivers are limited in terms of the types of variables they can perceive well. For example, humans are capable of accurately estimating visual angles encompassing the leader vehicle, time-to-collision (TTC) (visual angle divided by rate of change in visual angle) [18]. They are ill-suited to estimate distances; especially longitudinally- and absolute velocities and differential velocity to the leader vehicle; whereas the radar and laser measure these parameters well. The absolute signals, space headway (ΔY), differential velocity (Δv), and velocity (v_f), can be used to calculate the TTC.

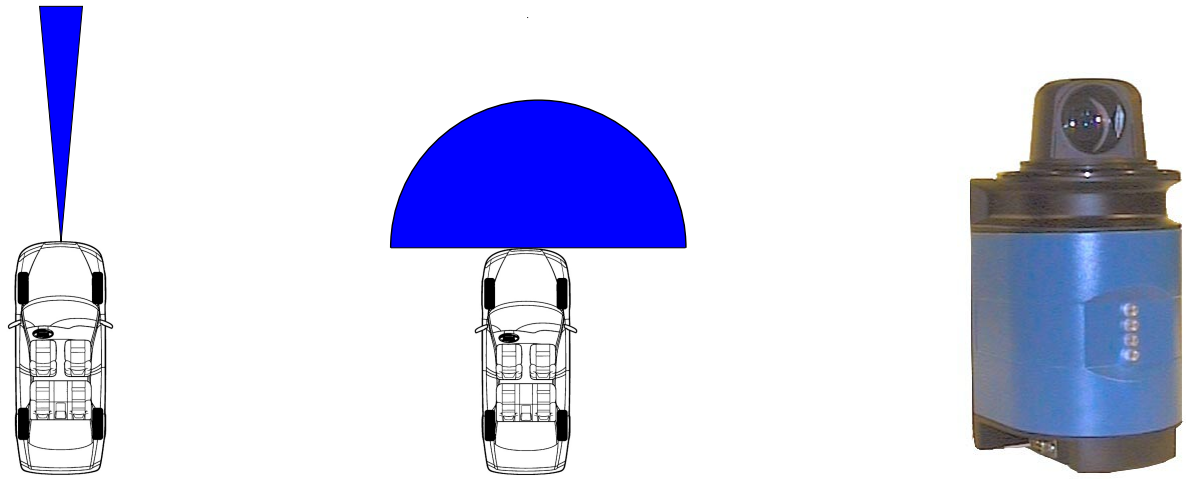

Figure 3.2 Radar (left) and laser (middle) mounted on vehicle. The used laser from IBEO (right).

Data were collected with a sampling rate of 10Hz. The measured variables were space headway (ΔY), differential velocity (Δv), velocity (v_f), throttle angle (α_t) and brake pressure (p_b). The measured α_t is the control signal to the throttle servo, not the actual throttle position. However, since the actual throttle position is almost proportional to the measured α_t, it can be viewed as the throttle position in a different scale. The measured p_b is the set-point to the braking system. Several experiments showed that in practice this difference could be neglected and therefore the measured α_t and p_b were treated as measurements of actual values.

The vehicles used in the experiment were not equipped with an accelerometer or GPS. However, both vehicles were equipped with a CAN bus, which was used for acquisition of measurements.

3.3 Experimental design

Fig. 3.3 shows a car following situation. The velocity of the leader vehicle and the follow vehicle are denoted v_l and v_f respectively, and the distance between the vehicles are denoted ΔY, where headway

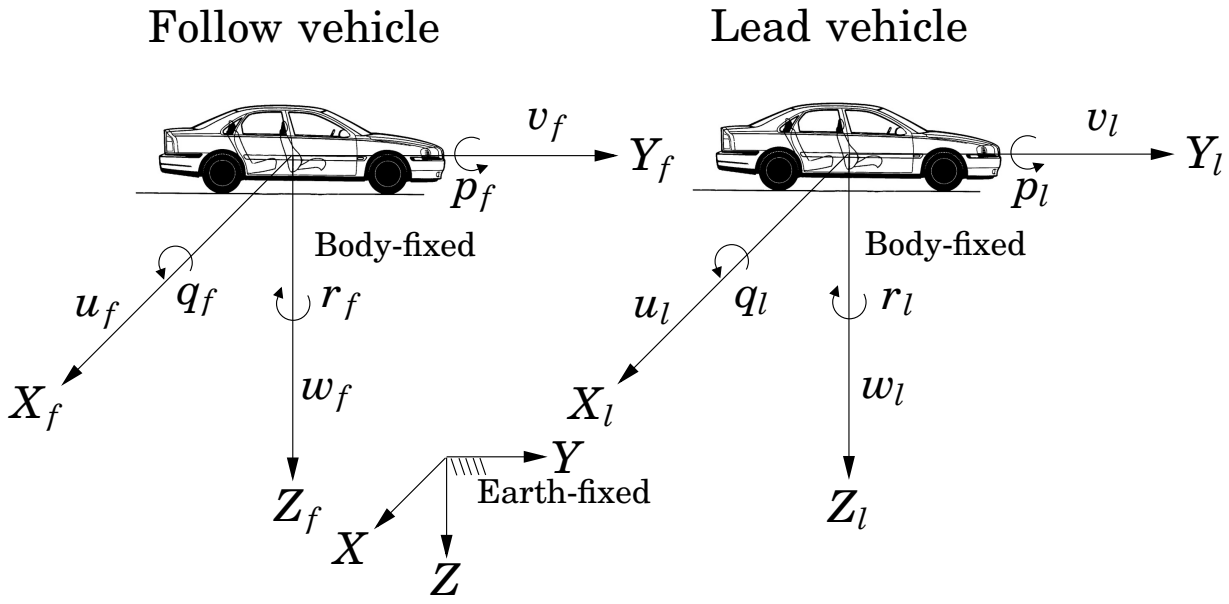

Figure 3.3 Body-fixed and earth-fixed reference frames.

$\Delta Y = y_l - y_f$. The relative speed is defined as:

$$\Delta v = v_l - v_f = \frac{d}{dt}\Delta Y \tag{3.1}$$

The driver's longitudinal behavior changes in different traffic situations. Therefore, in order to study the driver behavior, it is necessary to design experiments which capture driving behavior in standard traffic situations:

- **Free flow:** In the free flow situation the driver is uninfluenced by other cars, and attains his desired speed.
- **Follow:** The follow situation describes a scenario where the driver follows the leading vehicle and tries to maintain a desired individual headway distance.
- **Cut-in:** The cut-in situation describes a scenario wherein a vehicle cuts in in front of the driver's vehicle from a different lane. During this scenario the minimal individual headway distance can be exceeded for a short period in order to maintain driving comfort. The cut-in vehicle could have a higher speed or a lower speed than the driver's vehicle.

- **Braking:** In a braking situation, the headway distance decreases below the individual minimal headway distance, and the driver brakes to reestablish the headway distance.
- **Approaching:** In an approaching situation the driver is closing up behind the front vehicle and starts to adjust his speed to the vehicle in front. During this situation the driver change from free flow driving to car following.

Follow situations

The Follow situation data were collected for 8 different experiments, performed on public roads as well as on a test track. Six of these experiments were performed on two lane public roads and the velocity was in the range of 65 to 90 km/h. The experiments were designed to mimic free way and main country road environments. The velocity of the leader vehicle changes smoothly, without fast accelerations. Two of these experiments were performed on a two-lane test track and the velocity was in the range of 0 to 55 km/h. The experiments were designed to mimic urban environment and included some stop-and-go situations. The velocity of the leader vehicle in urban situations can change fast which was taken into account during the design of the experiments.

As well known, human drivers differ in their behavior, each driver having his own driving behavior, different desired headway distance, more or less aggressive, etc. To study the driving behavior it is desirable to be able to repeat exactly the same experiment for each test person who participated in the study. This was achieved since the used leading vehicle in the study was equipped with a system allowing control of the brakes and of the throttle. The experiment was then performed in the following way.

- The kind of situation was decided (country side/urban).
- The road and length of the experiment were chosen.
- The vehicle which was used as the leader vehicle in the experiment was used to drive the chosen road part and the brake pressure and throttle angle were measured and stored.

The leader vehicle had the property of being programmable to drive along a predefined longitudinal trajectory, which was specified using

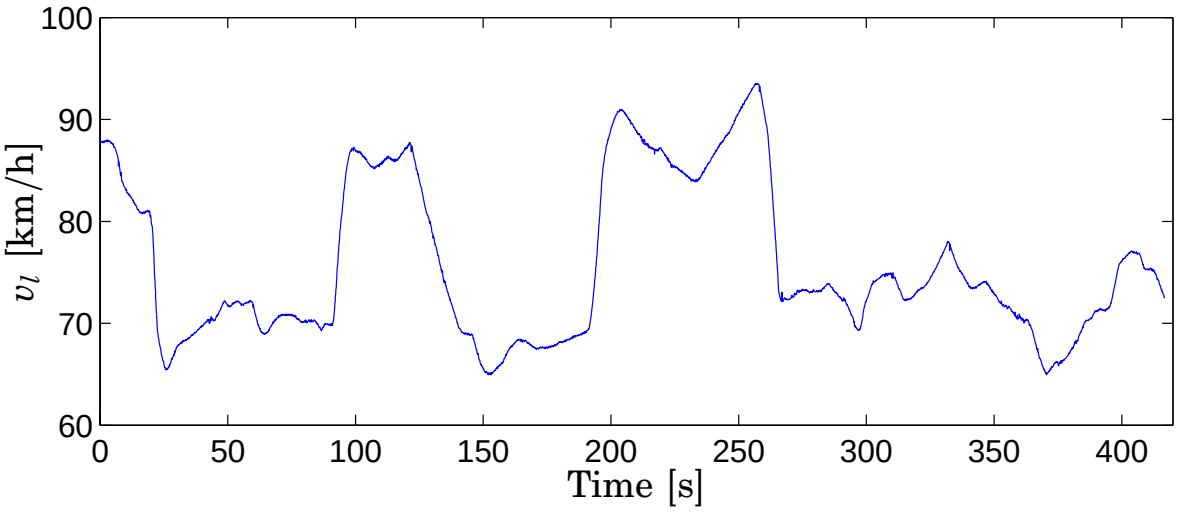

Figure 3.4 Velocity of the leader vehicle in one of the follow situations.

brake pressure and throttle angle. This programmability was used to repeat the experiment for several drivers while simulating the same traffic situation. This minimized influence from unknown factors, resulting in a simpler comparison between driver behaviors. The participating drivers in the experiments drove the follow vehicle and tried to maintain the individual desired following distance. The length of the experiment on the public roads was around 10km and that of the ones carried out on the test track was around 2km.

Cut-in situations

The following cut-in situations were performed both on public road and on a test track.

In order to make the experiment similar for all drivers, three different cut-in distances were specified: short, medium, and far (Tables 3.3 and 3.4). The short distance was chosen closer than minimal headway distance so that the driver must perform noticeable brake action immediately. The medium distance was chosen close to the minimal headway distance so that the driver could allow short exceeding of the headway distance, but still the driver needed to perform some braking action. The far distance was chosen near the maximal headway distance such that the driver would only need to reduce the throttle

V_{leader} (km/h)	$V_{follower}$ (km/h)	$\Delta distance$ (m)
40	50	short
40	50	medium
40	50	far
50	50	short
50	50	medium
50	50	far
60	50	short
60	50	medium
60	50	far
60	70	short
60	70	medium
60	70	far
70	70	short
70	70	medium
70	70	far
80	70	short
80	70	medium
80	70	far
80	90	short
80	90	medium
80	90	far
90	90	short
90	90	medium
90	90	far
100	90	short
100	90	medium
100	90	far

Table 3.3 Experimental protocol of cut-in situations.

V_{leader} (km/h)	$V_{follower}$ (km/h)	$\Delta distance$ (m)
90	110	short
90	110	medium
90	110	far
100	110	short
100	110	medium
100	110	far
110	110	short
110	110	medium
110	110	far

Table 3.4 Experimental protocol of cut-in situations.

angle. The situations where the driver drove in 70 or 90 km/h were carried out on public road and the situations where the driver drove in 50 and 110 km/h were carried out on a test track. The driver was either in following or free flow mode when the cut-in occurred.

Braking situations

The following braking situations were performed on both public road and a test track. Three types of braking situations where tested.

Type 1: When the braking situation starts, the driver is in following mode and tries to maintain the desired headway distance. The leader vehicle had the property of being able to set the deceleration to -3, -4, or -5 m/s^2, which allowed the different drivers to perform the same traffic situation. In the experiments the leader vehicle brakes to a final velocity and then maintains this velocity (Tables 3.5 and 3.6). The driver thereafter changes back to following mode.

Type 2: When the braking situation starts, the driver is in approaching mode but would soon switch to following mode. In the experiments the leader vehicle brakes to a final velocity and then maintains this velocity (Table 3.6). The driver thereafter changes back to following mode.

Type 3: When the braking situation starts, the driver is in following mode. In the experiments the leader vehicle brakes to zero velocity and

V_{leader} (km/h)	$V_{follower}$ (km/h)	a (m/s^2)	V_{leader} final (km/h)
50	50	-3	20
50	50	-4	20
50	50	-5	20
60	60	-3	30
60	60	-4	30
60	60	-5	30
90	90	-3	50
90	90	-4	50
90	90	-5	50

Table 3.5 Experimental protocol of braking situations.

V_{leader} (km/h)	$V_{follower}$ (km/h)	a (m/s^2)	V_{leader} final (km/h)
110	110	-3	70
110	110	-4	70
110	110	-5	70
V_{leader} (km/h)	$V_{follower}$ (km/h)	a (m/s^2)	V_{leader} final (km/h)
50	60	-3	20
50	60	-4	20
50	60	-5	20
70	90	-3	50
70	90	-4	50
70	90	-5	50

Table 3.6 Experimental protocol of braking situations.

the driver stops (Table 3.7).

Approaching situations

The following approaching situations were performed on a test track.

When the experiments start the driver is approaching the leading

V_{leader} (km/h)	$V_{follower}$ (km/h)	a (m/s^2)
50	60	-3
50	60	-4
50	60	-5
70	90	-3
70	90	-4
70	90	-5

Table 3.7 Experimental protocol of braking situations.

V_{leader} (km/h)	$V_{follower}$ (km/h)	
60	70	90
80	90	110

Table 3.8 Experimental protocol of approaching situations

vehicle and the experiments are finished when the driver switched to following mode (Table 3.8).

Free flow

Free flow was not studied since the purpose of this thesis was to study and model the driver longitudinal behavior in cases with a leading car present.

All experiments were repeated twice in order to study divergence in the behavior. Seven different drivers of various age (23–35), six men and one woman, participated in the data collection. The data acquisition was performed in the summer of 2000 during good weather conditions.

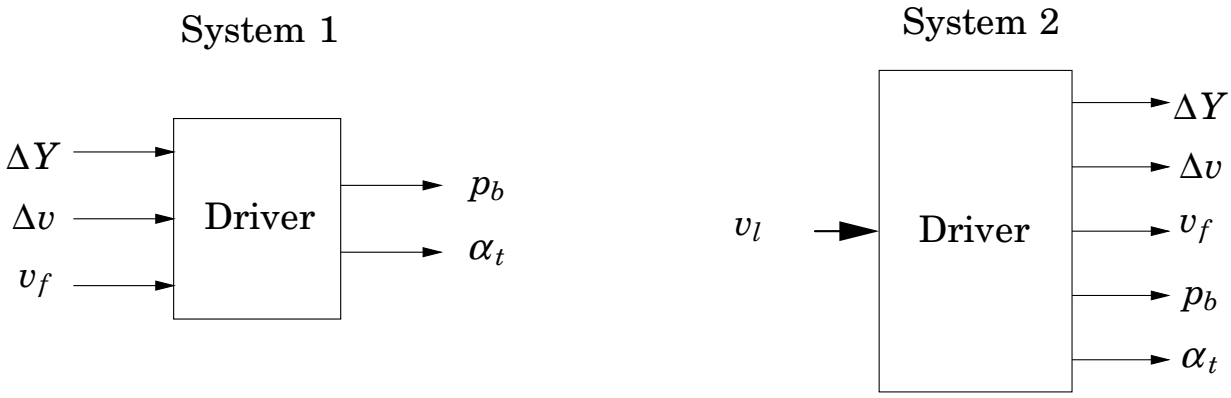

Figure 3.5 Representations of two different input and output separations. System 1 is the standard separation.

3.4 System identification

Data Analysis

There are at least two possible separations of input and output variables, the first one being the selection ΔY, Δv, and v_f as inputs and the outputs as α_t, p_b (Fig. 3.5). This is the standard separation. The other approach is to let the velocity of the leader, v_l be the input and ΔY, Δv, v_f, α_t, and p_b to be the outputs (Fig. 3.5). This model is useful since there is interaction between the driver and the vehicle.

Figs. 3.6 and 3.7 show data from one of the following situations in which the seven drivers participated. There are individual differences among the drivers, but also large similarities among their behaviors. The major differences between the drivers consist in the choice of space headway and safety distance. Some of the drivers drove with caution and kept a long headway distance. These drivers only used small brake pressure. Those drivers who drove more aggressively and kept a short headway distance used higher brake pressure.

Fig. 3.8 shows data from cut-in situations. In the cut-in situation the driver allowed the headway to distance decrease below the individual minimal headway distance for a short period in order to avoid unnecessary hard deceleration. After a while the headway distance stabilizes around the individual headway distance. There are similarities in their behavior, the drivers allow the headway distance to be reduced

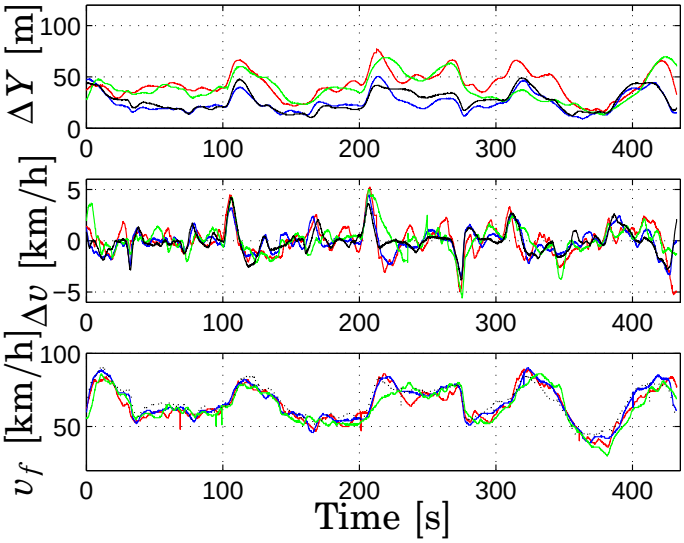

Figure 3.6 Data collection from of the inputs in one following situation. Data were collected from different drivers.

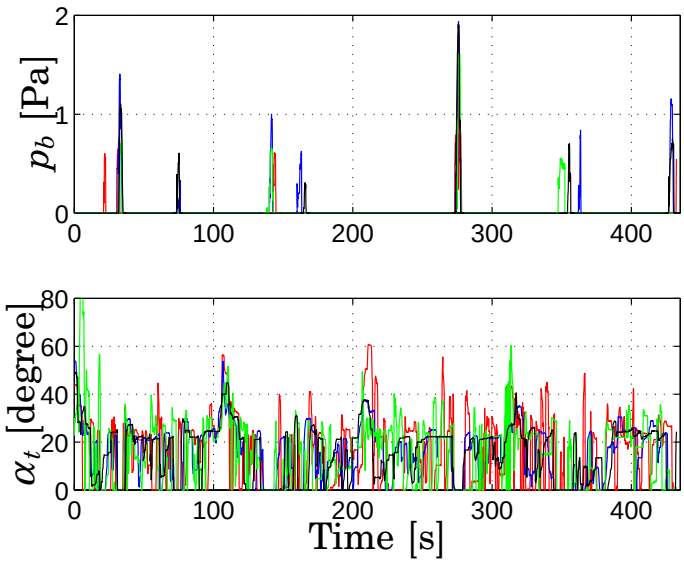

Figure 3.7 Data collection from of the outputs in one following situation. Data where collected from different drivers.

far below the desired headway distance in order to avoid hard deceleration. How far below the headway distance was allowed to be reduced to and how quickly the desired headway distance was reestablished differ between the drivers.

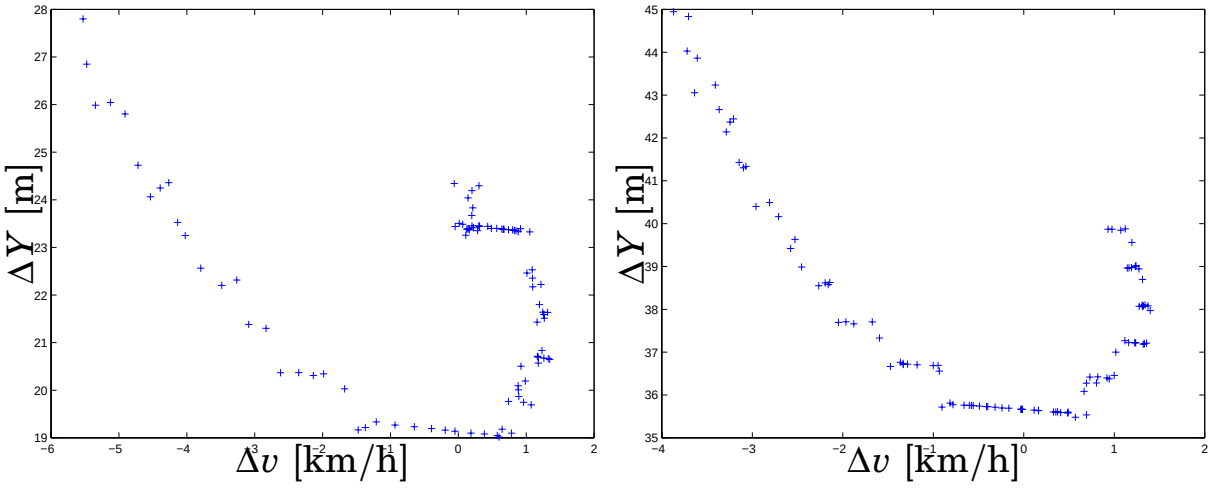

Figure 3.8 Data collection from two different cut in situations ($\Delta v \Delta y$-plane).

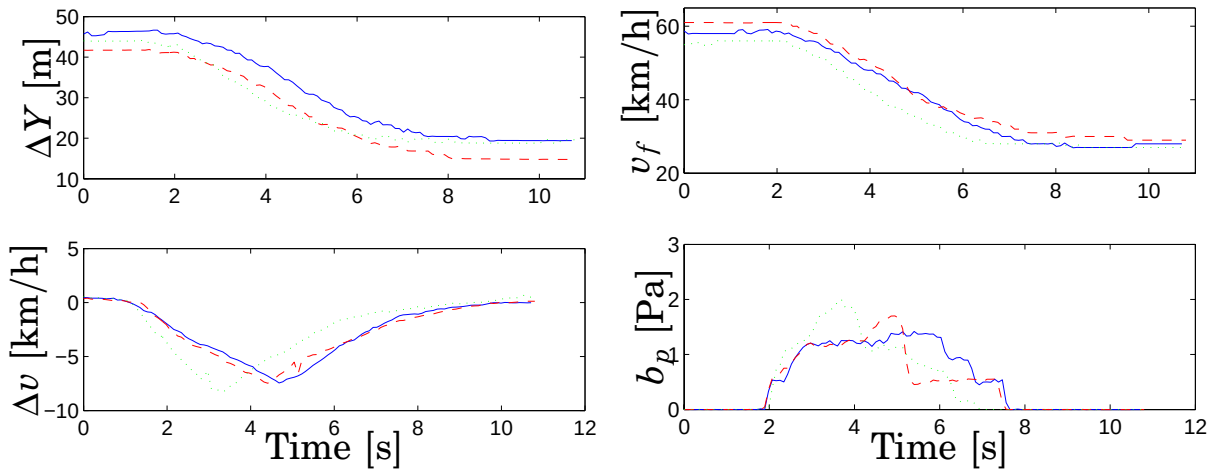

Figure 3.9 Data collection of a brake situation. ΔY (*upper left*), Δv (*lower left*), v_f (*upper right*), and b_p (*lower right*).

Fig. 3.9 shows data from two brake situations. When the sequence starts the drivers keep the individual headway distance. Then the leader vehicle brakes with -5 m/s^2 from 60 to 30 km/h. Fig. 3.10 shows how the two situations look like in the $\Delta v \Delta Y$-plane. They differ from the behavior in cut-in situations.

There are similarities, but the brake pressure profiles differ, for instance the cautious driver uses early high brake pressure in order to rapidly settle the desired headway distance.

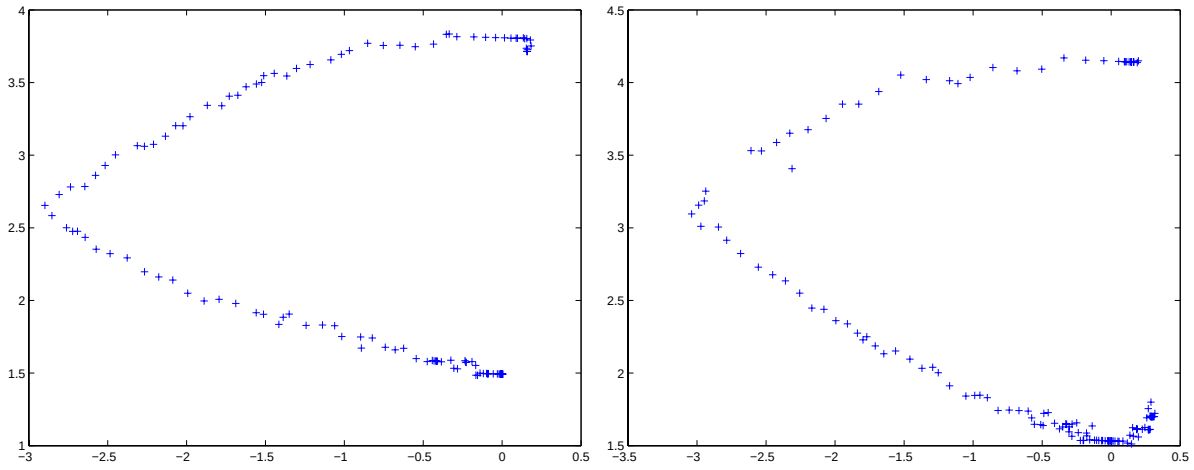

Figure 3.10 Data collection from two different braking situations ($\Delta v \Delta Y$-plane).

Fig. 3.11 shows data from an approaching situation where the driver changed his behavior from free flow mode to following mode. When the situation started the driver drove in free flow mode and then caught up with a leader vehicle and started to adjust his speed to the vehicle in front. In the end of the sequence the driver tried to maintain his desired headway distance. Different drivers start to adjust the velocity to the vehicle in front at different moments. Some start early to adjust the speed and uses a long time to catch up with the vehicle and to switch to following mode, others start later and use shorter time to catch up.

Data analysis was done by means of system identification methodology [28]. Auto-spectra, cross-spectra and coherence spectra of the inputs (ΔY, Δv, and v_f) and outputs (α_t and p_b), were made for assessment of the various signal levels and relationships. In Fig. 3.12 the estimated transfer function of the drivers from a car-following situation is shown. A rectangular window with the same length as the data series was used. Since the used data series where long, 4600 or more data points, the ringing effects are small and the purpose is not to examine two contiguous sinus frequencies. The transfer functions were calculated for 512 frequencies.

Some similarities between the estimated transfer functions of the drivers can be observed. The amplitude of the estimated transfer func-

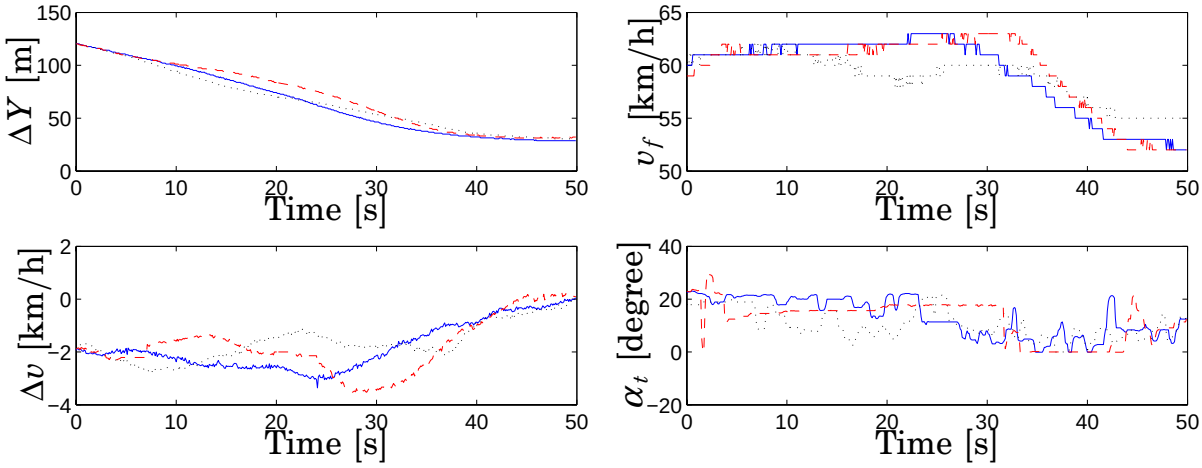

Figure 3.11 Data collection of a approaching situation. ΔY (*upper left*), Δv (*lower left*) v_f, (*upper right*), and α_t (*lower right*).

tions between the input ΔY and the output b_p show for all driver derivation effects for low frequencies. Apparently, there are zeros in the transfer function for higher frequencies. The phase of the estimated transfer functions between the input ΔY and the output b_p shows that there is time delay among the drivers, i. e., the reaction time. It is hard to estimate the time delay well using spectral analysis. The result depend on window size, window type. The properties of the model could drastically change when modifying, for example, the window size. From estimated transfer functions using rectangular window with the same size as the data series it was found that the reaction time among the drivers varies in the interval 1.3 to 4.4 s. When using a Hamming window with the length 256 it was found that the reaction time among the drivers varies in the interval .25 to 1.3 s. Thus, failure to find consistent estimations leaves doubts on the usefulness of spectrum analysis. Another approach is to estimate a high order linear model and study the transfer function. In Fig. 3.12 an estimated transfer function between ΔY and α_t using a high order prediction error estimate of a general linear model is shown. Also here we notice that the phase lag is large for high frequencies indicating a time delay. The amplitude curve shows bandpass properties. Fig. 3.13 shows the transfer functions between the inputs and the outputs for one driver in a following situation, where the model is a high order

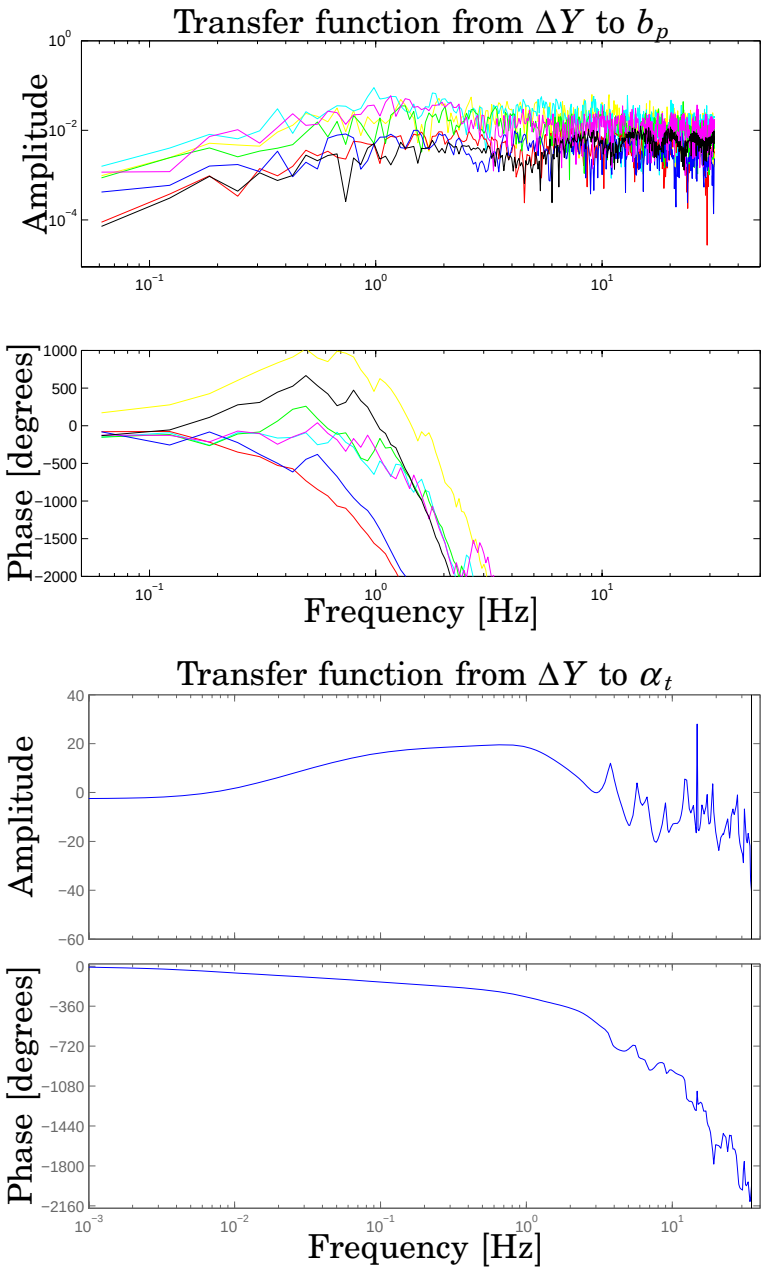

Figure 3.12 Estimated transfer function between ΔY and b_p using spectrum analysis (*upper*), each line in the plots corresponds to one driver. Estimated transfer function between ΔY and α_t using a high-order prediction error estimate of a general linear model (*lower*), one driver.

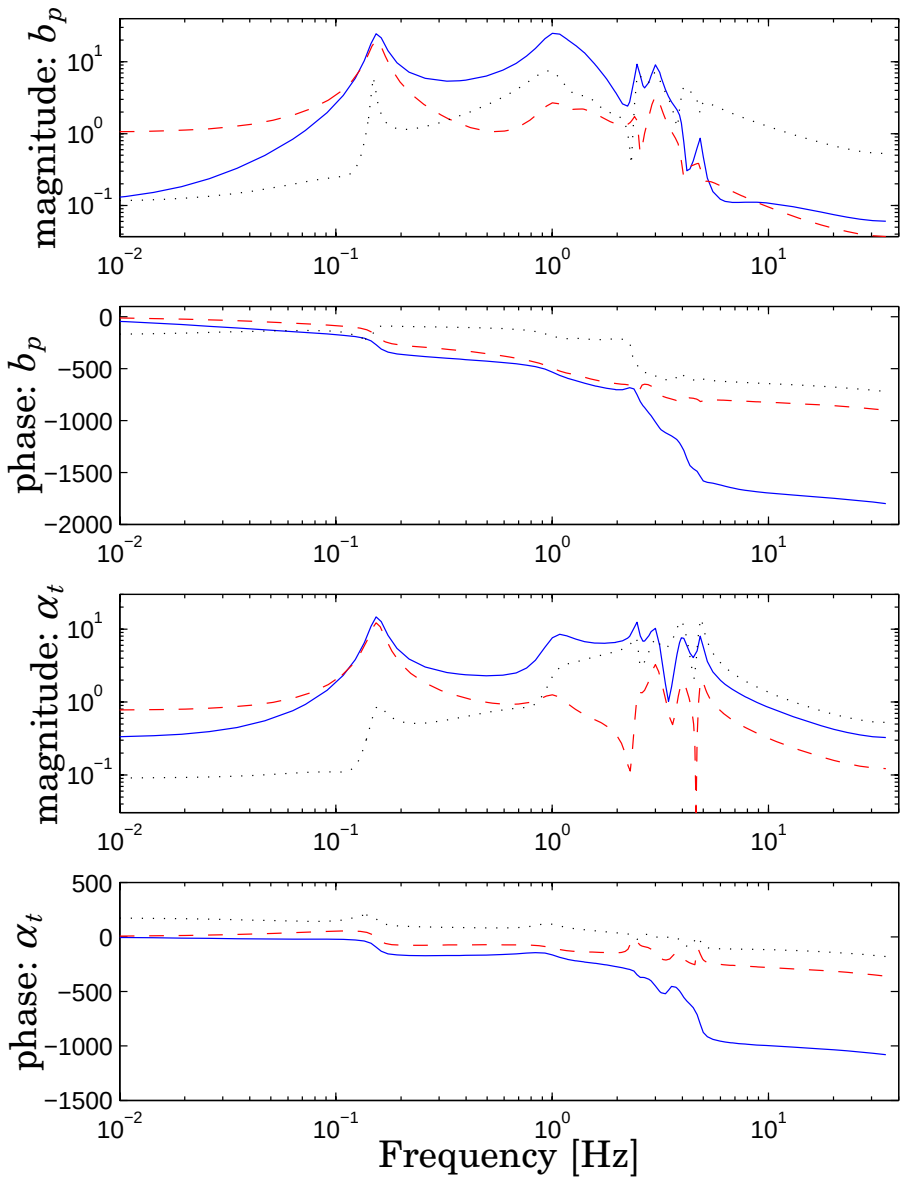

Figure 3.13 Estimated transfer function, using a high-order subspace model, between ΔY and b_p (*solid*), and Δv and b_p (*dashed*), and v_f and b_p (*dotted*) (*upper*). Estimated transfer function, using a high-order subspace model, between ΔY and α_t, and Δv and α_t (*dashed*), and v_f and α_t (*dotted*) (*lower*).

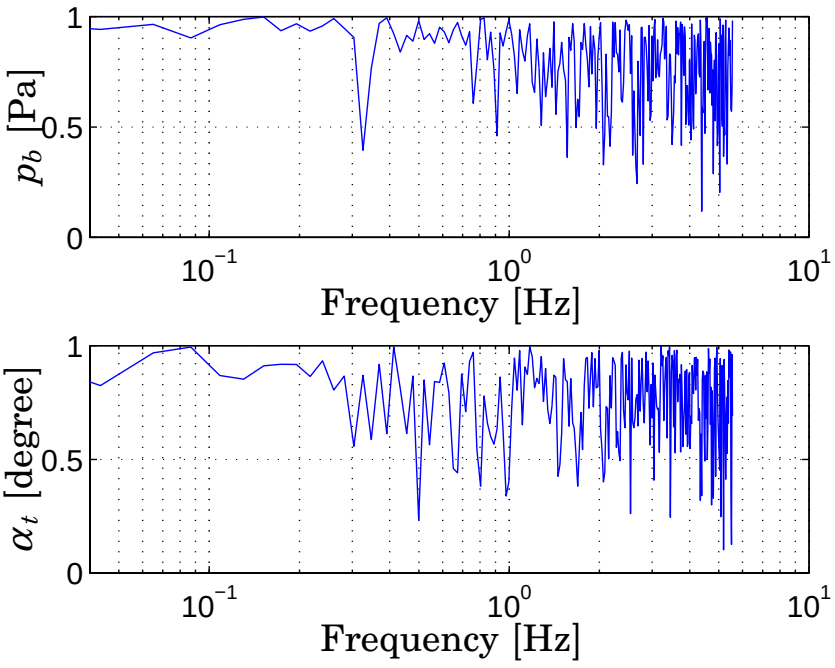

Figure 3.14 Coherence spectra between the inputs and the outputs. The upper figure: coherence between inputs $[\Delta Y \quad \Delta v \quad v_f]$ and the output p_b. The lower figure: coherence between inputs $[\Delta Y \quad \Delta v \quad v_f]$ and the output α_t.

state space model estimated using the subspace method. The driver proves to have bandpass properties and this is also what we would expect, since it has been found elsewhere that human sensors have bandpass properties [9].

Drivers use the throttle in a different manner than the brakes. The throttle is almost continuously used and often the changes are slow. The brakes are seldom used and changes can be fast or slow. The reaction time is best estimated using braking situations. Drivers plan the usage of the throttle using the assumption that if no obstacle is seen the leader vehicle will keep the current velocity. This could explain some of the differences between the b_p and the α_t.

In Fig. 3.14 the coherence spectra among inputs and outputs are shown. All the three signals ΔY, Δv, and v_f were used as inputs. The coherence among inputs and outputs is high, which can be interpreted as an indication that there exists a linear relationship between the inputs and the outputs. Note that the coherence for p_b is higher than

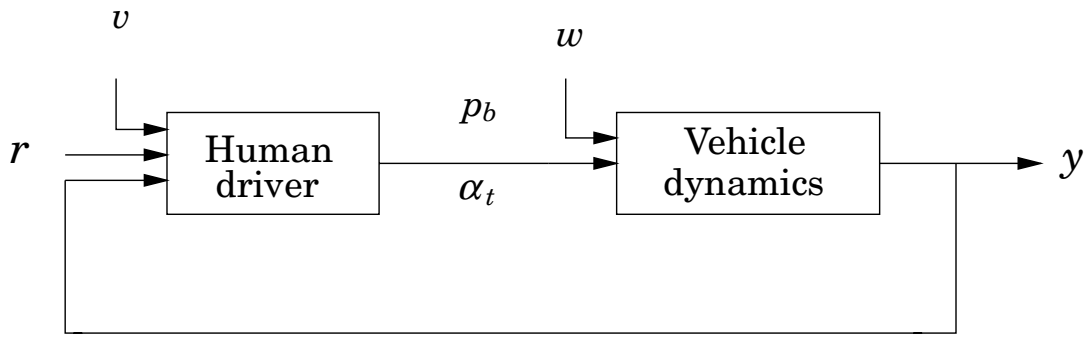

Figure 3.15 Structure of a human driver in car-following with r as the inputs to the driver from the lead vehicle, v as the observation noise, w as the motor noise, and y as the car position and velocity.

for α_t.

System identification and modeling methods

Interaction of the car and the human driver can be viewed as a closed-loop system with feedback from the front vehicles velocity v_l (Fig. 3.15). All the experiments were performed in closed-loop feedback operation and there may be systematic problems how to obtain relevant information from this type of experiments [28, Ch. 8]. If there is feedback during the experiment, the data may not be informative enough to establish a valid model of the driver. The system is of multi-input multi-output structure.

We use the inputs and outputs chosen to make a direct identification of the human driver. Different models have been used which, in short is described below.

Linear regression models To find out if there is some relationship between the input data and the output, a linear regression model was estimated [28]. The linear regression model takes on the format

$$y_k = [\Delta Y_k ... \Delta Y_{k-n} \; \Delta v_k ... \Delta v_{k-n} \; v_{f_k} ... v_{f_{k-n}}] \, \theta + e_k \tag{3.2}$$

where n is the estimated order and e_k represents an additive error sequence. A linear regression model of high-order was estimated. Since the model order is high, it may be assumed that the computed residual $\varepsilon_k = y_k - \hat{y}_k$ is a good approximation of the noise e_k. The computed

residual sequence was used in pseudolinear regression to estimate a model of lower order. This method is also known as a two-step linear regression approach.

State-space models using subspace-based identification A discrete-time time-invariant system in state-space realization: Innovation model

$$\begin{aligned} x_{k+1} &= Ax_k + Bu_k + Kw_k \\ y_k &= Cx_k + Du_k + w_k \end{aligned}$$

where w_k and v_k are noise sequences. The problem is to estimate the order n of the system and the system matrices A, B, C, D. In Fig. 3.16 there is a schematic representation of the identification problem. The

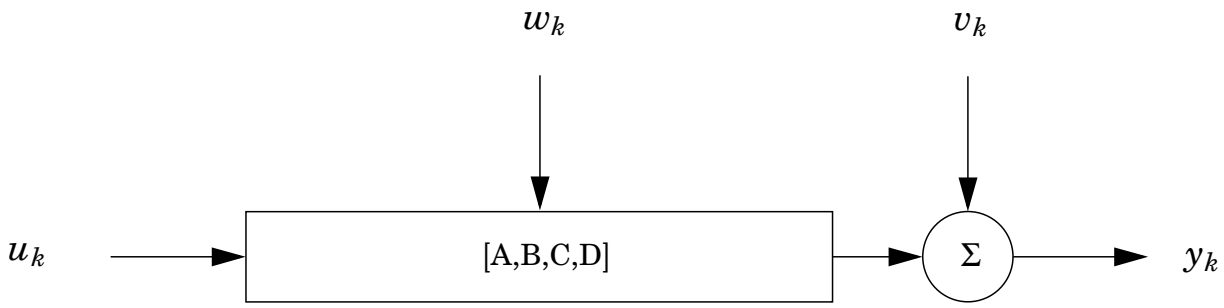

Figure 3.16 Schematic representation of the innovations model identification problem.

subspace method is well suited for modeling of multivariable systems [28]. To determine the order, a Hankel matrix is constructed [51, 50]. The choice of model order is based on the singular values of the Hankel matrix. However, if there is strong noise influence then this criterion degrades and becomes non-conclusive.

Behavioral model Behavioral model identification may be suggested in cases without clear-cut distinction of signals as inputs or outputs [54, 29]. This may be preferable since there is feedback interaction between the driver and the car. There are also interactions between the driver and the other vehicles, for example in cut-in situations. The behavioral method has great similarities with the subspace method, but differs in its absence of explicit separation among inputs

and outputs. Thus, the estimated state-space model represents all the dynamics, both for the inputs and for the outputs. Then by matrix fraction description an input-output model can be obtained.

Detection of changed driver behavior The driver behavior depends on the traffic situation, it is therefore interesting to be able to detect changes in the behavior. One way to do this is to use a Generalized Auto-Regressive Conditional Heteroscedasticity, GARCH(r,m) model [8, 21].

An AR process of an order k is described as:

$$A(z^{-1})y_k = e_k \tag{3.3}$$

where e_k is white noise:

$$E\{e_k\} = 0 \tag{3.4}$$

$$E\{e_k e_i\} = \begin{cases} \sigma^2, & k = i \\ 0, & \text{otherwise} \end{cases} \tag{3.5}$$

The model could be used to predict the output y_k. Sometimes it is interesting not only to predict the output y_k, but also its variance. Heteroscedasticity refers to unequal variance in the regression errors, the variance changes over time. One approach is to model the amplitude varying residuals u_k^2 as an AR(m) process:

$$u_k^2 = \zeta + \alpha_1 u_{k-1}^2 + \alpha_2 u_{k-2}^2 + \cdots + \alpha_m u_{k-m}^2 + w_k \tag{3.6}$$

where w_k is a new white noise sequence:

$$E\{w_k\} = 0 \tag{3.7}$$

$$E\{w_k w_i\} = \begin{cases} \lambda^2, & k = i \\ 0, & \text{otherwise} \end{cases} \tag{3.8}$$

A process u_k satisfying 3.6 is called an autoregressive conditional heteroskedasticity (ARCH) process. An alternative representation is:

$$u_k = \sqrt{h_k} v_k \tag{3.9}$$

where v_k is white noise:

$$E\{v_k\} = 0 \quad E\{v_k^2\} = 1 \tag{3.10}$$

and

$$h_k = \zeta + \alpha_1 u_{k-1}^2 + \alpha_2 u_{k-2}^2 + \cdots + \alpha_m u_{k-m}^2 \tag{3.11}$$

The ACRH model can be extended into a generalized autoregressive conditional heteroskedasticity (GARCH) model which also includes lags of u_k^2.

$$h_k = \kappa + \delta_1 h_{k-1} + \delta_2 h_{k-2} + \cdots + \delta_r h_{k-r} + \alpha_1 u_{k-1}^2 + \alpha_2 u_{k-2}^2 + \cdots + \alpha_m u_{k-m}^2 \tag{3.12}$$

for

$$\kappa \equiv [1 - \delta_1 + \delta_2 + \cdots + \delta_r] \tag{3.13}$$

This could be used to model the behavior when the driver changes behavior in a traffic situation or due to the leader vehicle brakes or a vehicle cuts in when driving in following mode. Then the residual for a model designed for following mode becomes large, i.e., the driver diverge from following behavior.

3.5 Transposed data

Human drivers are difficult to model by linear models in their use of brakes and throttle. The throttle angle and the brake pressure are never less than zero and they are only piecewise active (Fig. 3.17). Using this fact, the result from the linear methods can be improved by transposing the resulting negative brake pressure to positive throttle angle and negative throttle angle to positive brake pressure. The transposed data is achieved by the following procedure:

- Estimate a model using normalized data;
- Simulate the estimated model;
- Truncate the data at zero level and move negative b_p to positive α_t and negative α_t to positive b_p.

Then the new transposed data provide acceleration-deceleration data, taking only positive values.. This is an attempt to improve the accuracy of the estimated models, and it proved to increase the result.

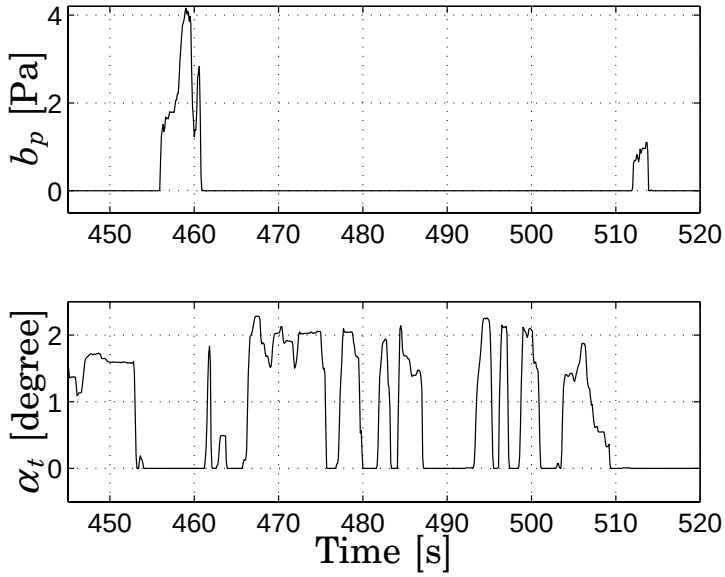

Figure 3.17 Normalized brake pressure and throttle angle from one driver in a follow situation.

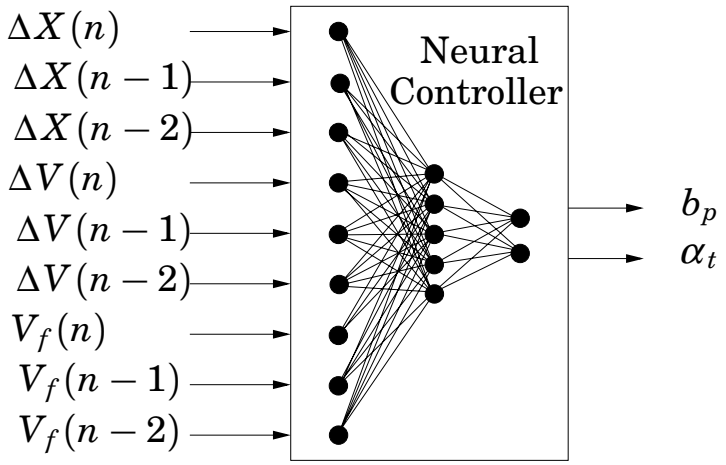

Figure 3.18 Neural controller with 9 input, 15 hidden, and 2 output neurons.

3.6 Driver modeling using neural networks

For comperative studies with the system identification approach neaural networks where trained. The data used for training consist of data from several sequences. Since a neural network consists of learning functional relationship between inputs and outputs it is possible to

combine several sequences to one, without affecting the dynamics. This makes it easier to train neural network in cut-in situations since these are only present during a short time interval. A cut-in situation usually only last for 30–40s and the collected data from one sequence is not enough to train a neural network. There exist several strategies for learning, in this study we have used back propagation [26]. There are many variations of the back propagation algorithm. The simplest implementation of back propagation updates the network weights and biases in the direction in which the gradient decreases most rapidly. The Levenberg-Marquardt algorithm [20] has been used for numerical optimization in all cases. All measured data have been scaled in such a way that all variables have the standard deviation 1. The neural network used for learning human driver behavior is shown in Fig. 3.18. The transfer function in the input and in the hidden layer was a hyperbolic tangent sigmoid transfer function. For the output layer it was purely linear.

Neural networks have been used for identification and modeling of driver's behavior. In the review some works in his field are mentioned. Human driver behavior can be described as the relationship between task inputs y and control outputs u. Neural network might be used in learning this functional relationship between y and u. One advantage of neural networks that it also can identify present nonlinearities. Unfortunately, one important drawback with trained neural networks is that they give no guarantee of closed-loop stability, i.e., when we use the trained model to act as a virtual driver. The neural network will be used in comparison to other models.

4

Validation & Results

4.1 Introduction

Different model structures have been designed and validated. The estimated models have been simulated in Matlab and in Simulink. In order to study the usefulness of different identification methods for the capturing of human driver behavior, a follow, a cut-in, and a braking situation were chosen and were used as test cases for all methods.

The follow situation involves two braking sequences, one larger and one smaller. The leader vehicle also made the driver to use the throttle actively during this sequence. The data is from one of the follow situation and the total length of the situation is around 7 minutes. In the estimation of the model all 7 minutes of data were used.

By studying the correlation between α_t and acceleration, and between b_p and acceleration it was found that the brake and the throttle have different dynamic properties (Fig. 4.1). This is due to the fact that brake pressure affects the wheel almost directly, whereas the throttle only affects the carburetor air stream, which affects the combustion engine, which affects the transmission system, which finally affects the wheel.

Model validation was perfromed to verify whether the identified model fulfills the requirements of good model approximation properties. Methods used in the validation process were:

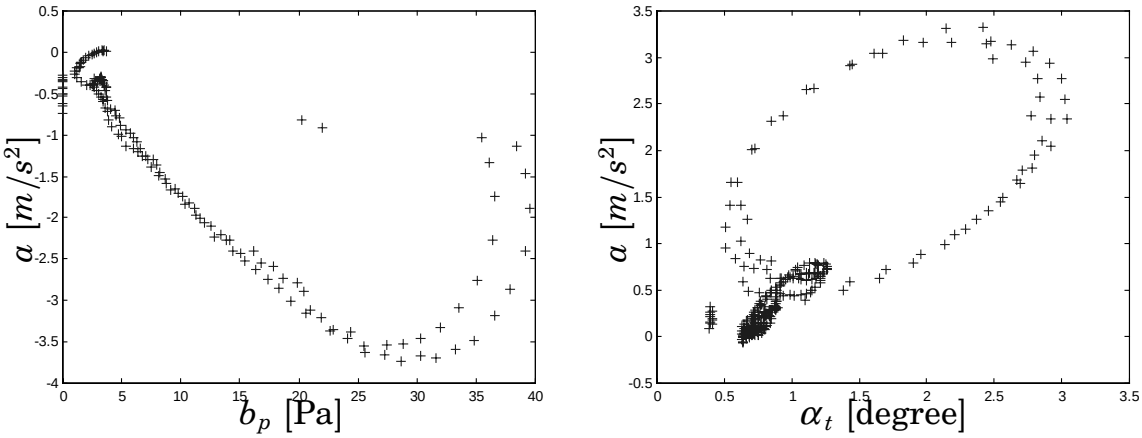

Figure 4.1 The static correlation between α_t (left) and b_p (right) and acceleration a.

- Variance-accounted-for (VAF);
- Residual analysis test;
- Cross-validation test.

Identification accuracy was measured using the Variance-Accounted-For (VAF)[28].

$$VAF = (1 - \frac{var(y - \hat{y})}{var(y)}) \times 100\% \tag{4.1}$$

The VAF score gives an identification of how close the original signal and its estimate resemble each other, both for bias and variance. If the VAF score is 100% they are complete equal.

The residuals is the misfit between real data and model data and residual analysis is useful when performing test of:

- Independence of residuals
- Normal distribution of residuals
- Zero crossings of the residual sequence
- Correlation between residuals and input

The cross-validation test, using data which not have been used in the identification procedure, is one of the most important validation tests. This test gives an indication whether the estimated model capture the dominated dynamics of the true system or not and if the model is able to predict the behavior when applied to new data.

In the model estimation the normalized ΔY, Δv, v_f, α_t and p_t were used. They where normalized with respect of the standard deviation.

4.2 Linear regression

For the linear regression model the inputs and outputs were chosen according to system 1 (Fig. 3.5). Linear regression models of different orders were estimated, but the regression models only succeeded to capture some of the driver behavior. Even if the order was increased, the result was not satisfying.

Follow situation

A linear regression model of order $n = 30$ is shown in Fig 4.2 for a follow situation. The model captures some of the driver behavior. The experiment setup is a closed-loop system, which makes the identification more difficult. The model is better in predicting the driver's throttle angle α_t behavior, than the brake pressure p_b behavior. A possible background would be that the acceleration and deceleration have different explanations, for example, that deceleration could be explained by air resistance or topography.

The residual analysis of the model is shown in Fig 4.3 and it was found that the residual from output α_t and from the output p_b have different distributions. This is probably due to the fact that the human drivers differ in their brake and throttle behavior. The coherence spectra between the chosen inputs and outputs were high, therefore we would expect better result from linear regression than obtained. One explanation could be that the brake pressure and the throttle angle are never less than zero and the throttle angle and the brake pressure are only piecewise active, and sometimes neither the brakes or the throttle are active. Composition of an acceleration signal from brake pressure and throttle angle may be suggested (Fig. 4.4). The signal composed

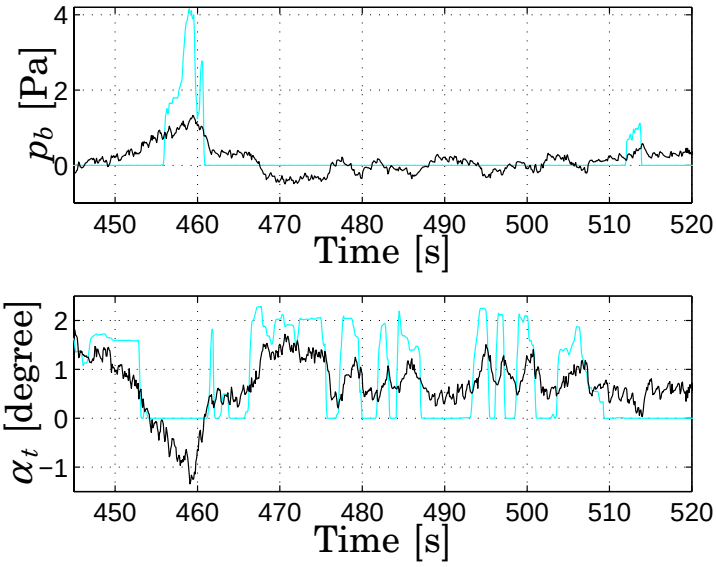

Figure 4.2 Measured b_p and α_t from one driver (*grey*) and simulated output data from a linear regression model of order $n = 30$ (*black*). Normalized brake pressure and throttle angle was used.

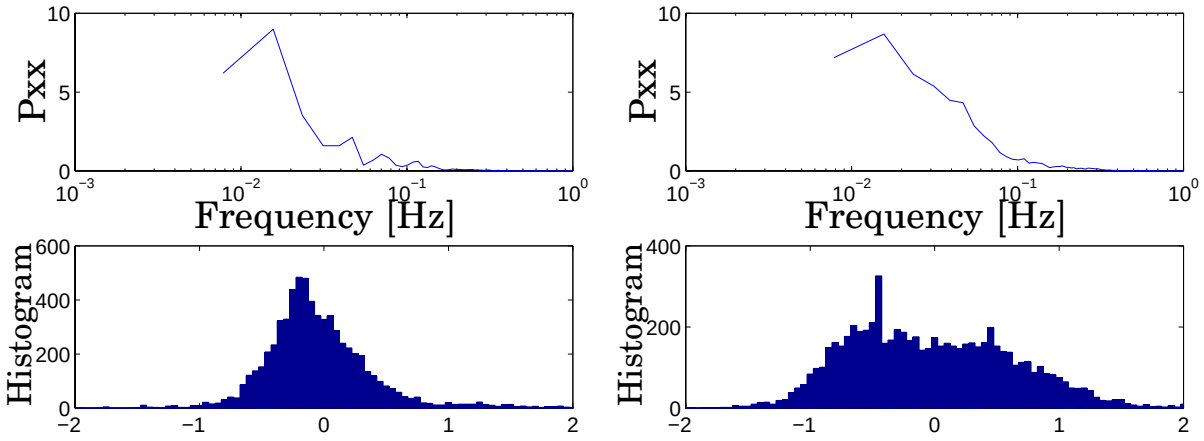

Figure 4.3 Histogram and auto-correlation of the residuals from a thirtieth order linear regression model. To the left is the residual of output p_b. To the right is the residual of output α_t.

was used as input but the result was not improved. The result from the linear regression model could be improved. The brake pressure and the throttle angle could only be positive. Consequently the negative contribution from the brake pressure could be transfered to the

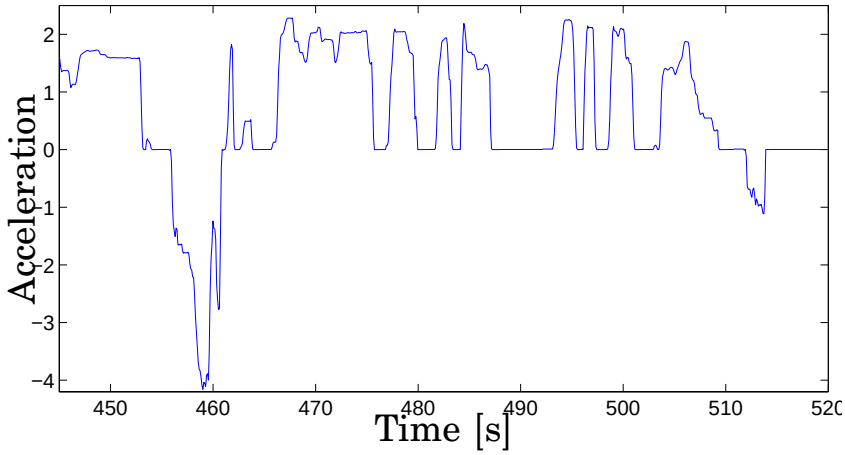

Figure 4.4 Acceleration as composed by normalized brake pressure and throttle angle. (arbitrary units)

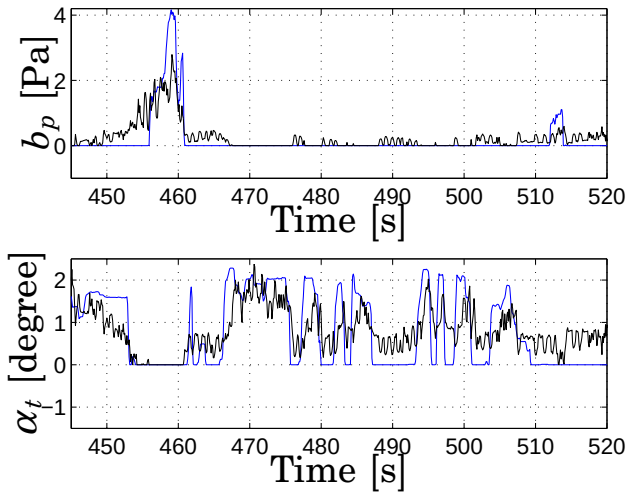

Figure 4.5 Measured b_p and α_t from one driver (*grey*) and simulated output data from a linear regression model of order $n = 30$ (*black*) when the negative contribution of brake pressure was transfered to throttle angle and vice versa. Normalized brake pressure and throttle angle were used.

throttle angle as positive and vice versa. The data are transposed into acceleration-deceleration signal (Fig. 4.5).

The residuals of this high order model were further used to estimate a pseudolinear regression model. The result is shown in Fig. 4.6, and the model captures most of the driver's behavior, even the braking behavior. The VAF scores for the linear regression model are 41.1% (p_b)

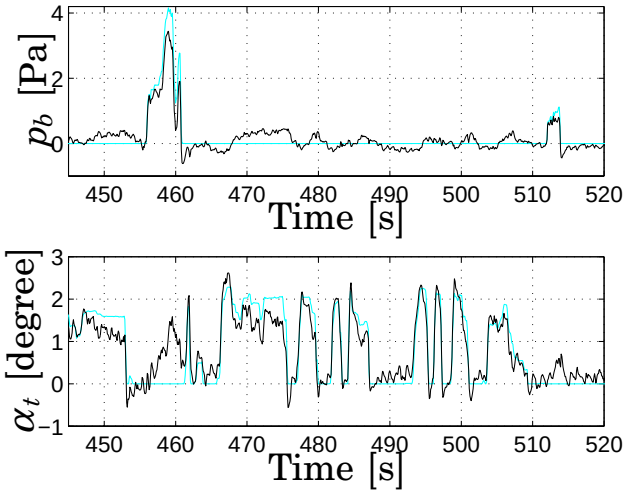

Figure 4.6 Measured b_p and α_t from one driver (*grey*) and simulated output data from a pseudolinear regression model of 3rd order (*black*).

and 46.2% (α_t) whereas the VAF scores for the linear regression model after transferring the negative contribution from b_p to α_t and vice versa, after the simulation of the model in acceleration-deceleration, are 52,7% (p_b) and 48.6% (α_t).

The VAF scores for the pseudolinear regression model are 89.9% (p_b) and 73.2% (α_t) respectively.

Cut-in situation

In Fig. 4.7 result from a 15th order model estimated by linear regression in a cut-in situation. The linear regression method have problem when using only a short period of data. Cut-in situations often only last for 8–13 s and the linear regression methods need longer data series to get good result. For this 15th order model 48 parameters are estimated and the total length of data series is 92. This will make the model over-fit and not robust against noise and in crossvalidation the model may give poor result. The VAF scores for the linear regression model are 94.5% (p_b) and 96.6% (α_t).

Brake situation

In Fig. 4.8 result from a 10th order model estimated by linear regression in a braking situation is shown. The result seems to be good. As

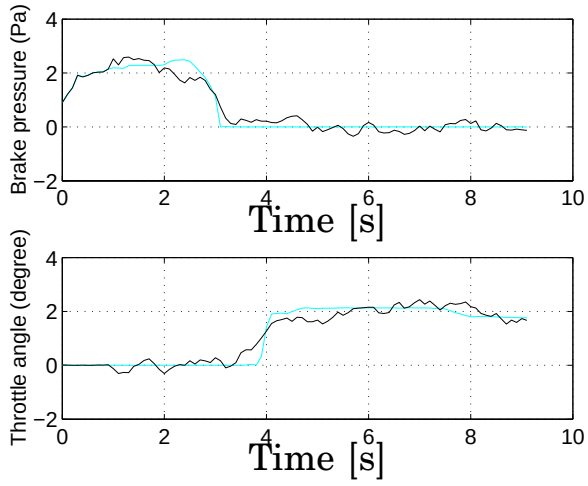

Figure 4.7 Cut-in: measured b_p and α_t from one driver (*grey*) and simulated output data from a linear regression model of 15th order (*black*).

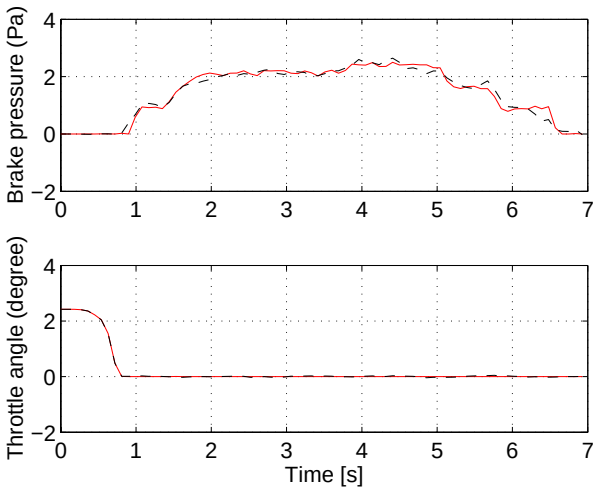

Figure 4.8 Brake: normalized b_p and α_t from one driver (*solid*) and simulated output data from a linear regression model of 10th order (*dashed*).

for the cut-in situations, the model tends to be over-fitted and not robust against noise. The VAF scores for the linear regression model are 97.4% (p_b) and 99.9% (α_t).

Approaching situation

In Fig. 4.9 result from a 15th order model estimated by linear regression in a approaching situation is shown. The approaching situation

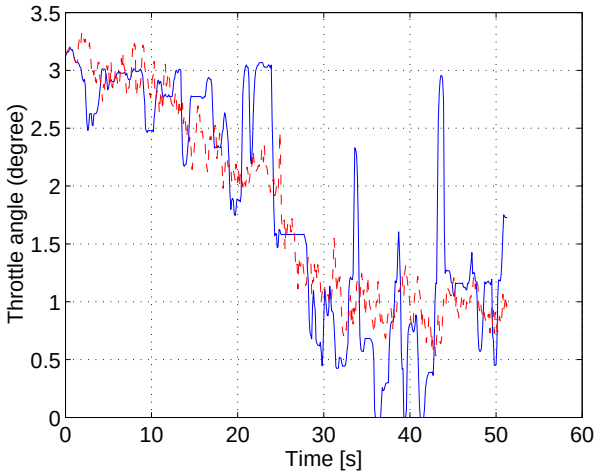

Figure 4.9 Approaching: normalized α_t from one driver (*solid*) and simulated output data from a linear regression model of 15th order (*dashed*).

does not involve any braking. Hence, only a model for the throttle behavior was estimated. The model only captures some of the driver behavior. The VAF scores for the linear regression model is 74,5% (α_t).

4.3 Subspace-based identification

In identification of state-space models by subspace-based methods input and output was chosen as system 1 (Fig. 3.5). The state-space models using subspace-based methods have been designed using the SMI Toolbox in Matlab [22]. State-space models of different orders were estimated. In Fig. 4.10 the result from a models of order $n = 5$ and and order $n = 15$ is shown. The estimated models capture some of the driver behavior. The result was better for the 15th order state-space model. The results from the state-space models were similar with the result from the 30th order linear regression model. The residual analysis of the model is shown in Fig. 4.11 and similar to the linear regression model the residual for α_t and p_b have different distributions. The estimated model $n = 15$ is better to capture the driver's throttle behavior than the brake behavior with VAF scores: 44.3% (p_b) and 48.7% (α_t). An estimated model $n = 5$ gives VAF scores of 30.3% (p_b) and 23.7% (α_t).

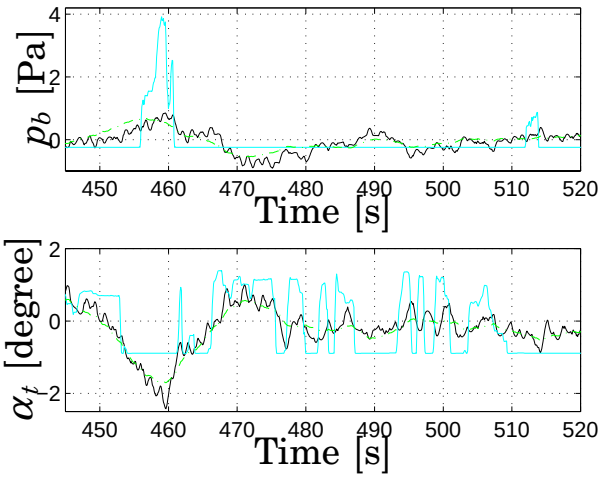

Figure 4.10 Measured b_p and α_t from one driver (*grey*) and simulated output data from state-space models using subspace-based methods, $n = 5$ (*dashdot*), and $n = 15$(*solid*). Normalized and detrended brake pressure and throttle angle was used.

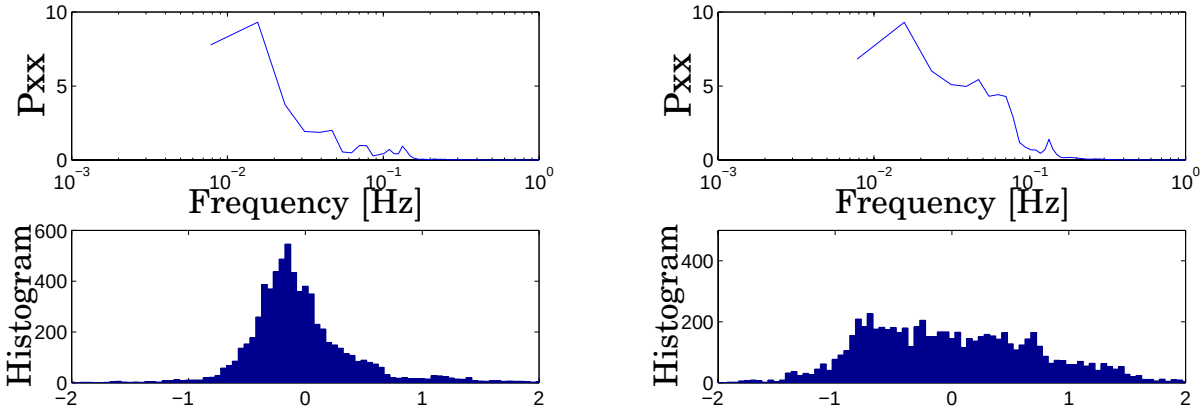

Figure 4.11 Histogram and auto-correlation of the residuals from a 15th order sub-space model. To the left is the residuals of output p_b. To the right is the residuals of output α_t.

The result from the estimated state-space model was improved by transposing data into a acceleration-deceleration signal. An attempt to transpose the data into acceleration-deceleration signal is shown in Fig. 4.12. The result for the 15th order estimated state-space model captures most of the driver behavior and we notice that a 5th order state-space model is not sufficient to capture the behavior. The VAF

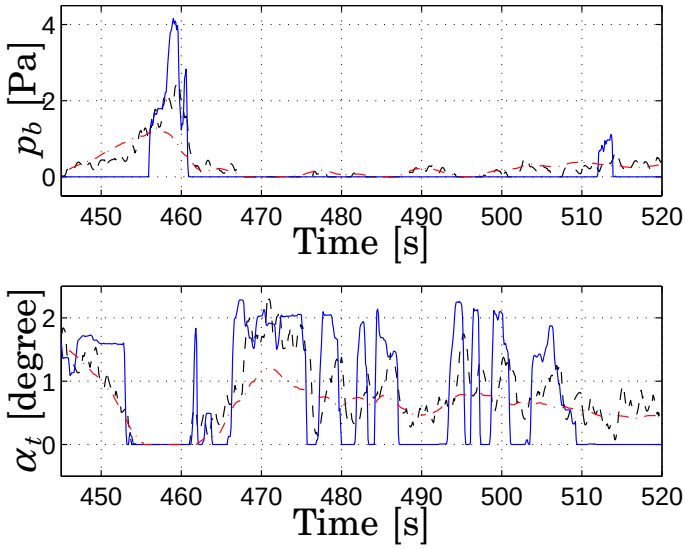

Figure 4.12 Measured b_p and α_t from one driver (*grey*) and transposed output data from state-space models using subspace-based methods, $n = 5$ (*dashdot*), and $n = 15$(*solid*). Normalized brake pressure and throttle angle was used. No transposed data were used in the model identification.

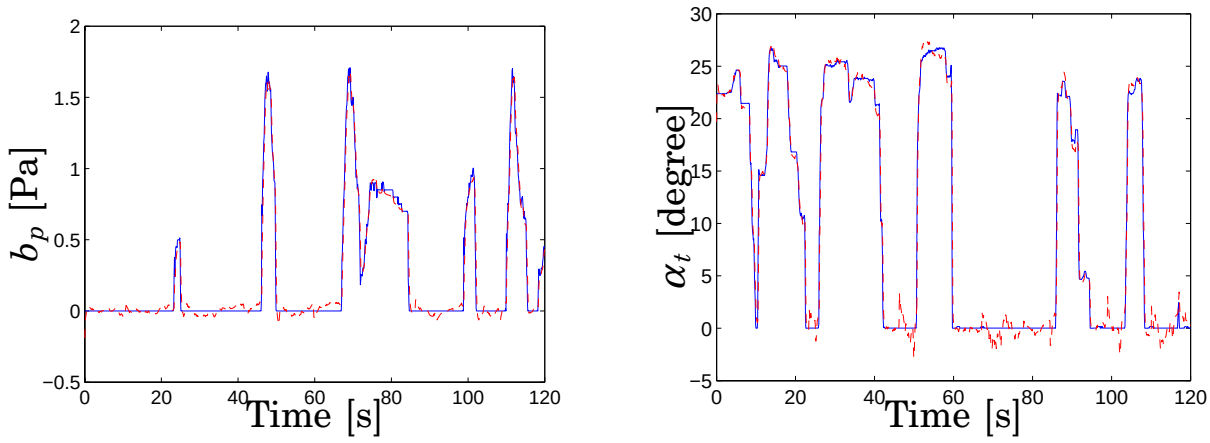

Figure 4.13 Measured b_p and α_t from one driver (*solid*) and simulated data from a one-step ahead predictor. (*dotted*).

scores after transposing the data are for the 15th order model are 55.5% (p_b) and 52.2% (α_t) and for the 5th order model are 42.3% (p_b) and 30.4% (α_t).

It is also interesting to study the results from a one-step predictor

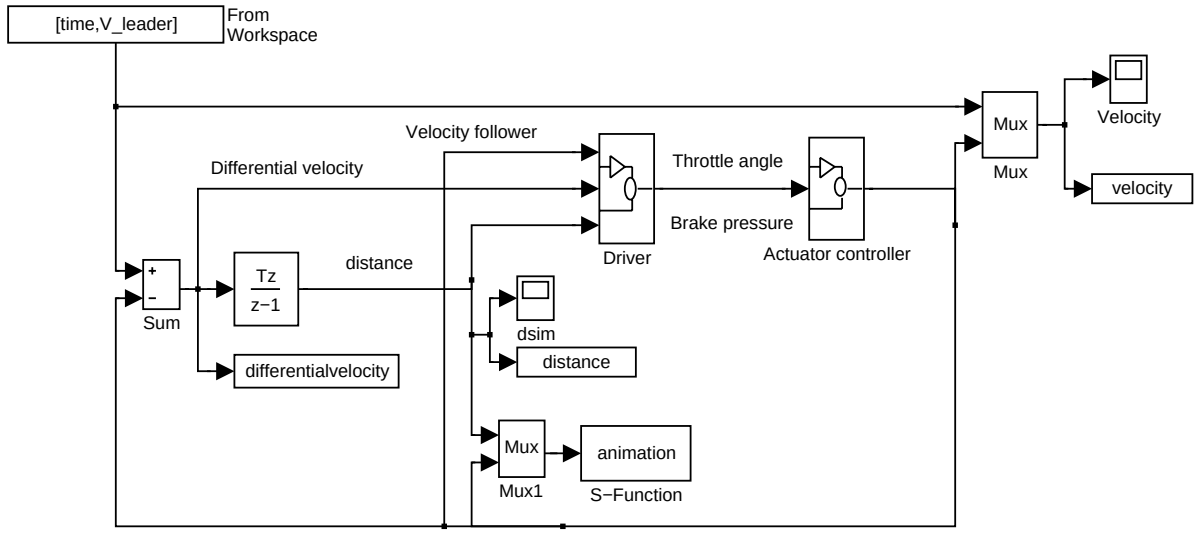

Figure 4.14 Simulink model of driver and actuator. Inputs to the model are: leading vehicle's velocity (v_l) and initial conditions, outputs are: ΔY, Δv and v_f.

using the estimated state-space models. Fig. 4.13 shows the result from a one-step predictor using the estimated 5th order. Even this low order model gives satisfying result, and the result can be improved by transposing the data.

Simulink models were designed in order to simulate and validate the estimated models, Fig. 4.14. The input to the Simulink model are leader vehicle's velocity (v_l) and initial conditions of the experiment, and the output are ΔY, Δv, and v_f.

In Fig. 4.15 the result from a Simulink simulation using a 7th order state-space model is shown: The follow vehicle succeeds in following the leading vehicle in a behavior similar to the driver, who was used in the experiment. In this simulation the data was not transposed into an acceleration-deceleration signal, which would improved the result. Nevertheless, the model captures most of the behavior. The input to the Simulink model was the velocity of the leader vehicle and the initial condition, that includes the headway distance of the follower at the start of the simulation. The input was the measured velocity of the leader in an urban follow situation which the participated drivers drove. It contains several stop situations and fast accelerations of the leader vehicle. The output from the simulation was compared with

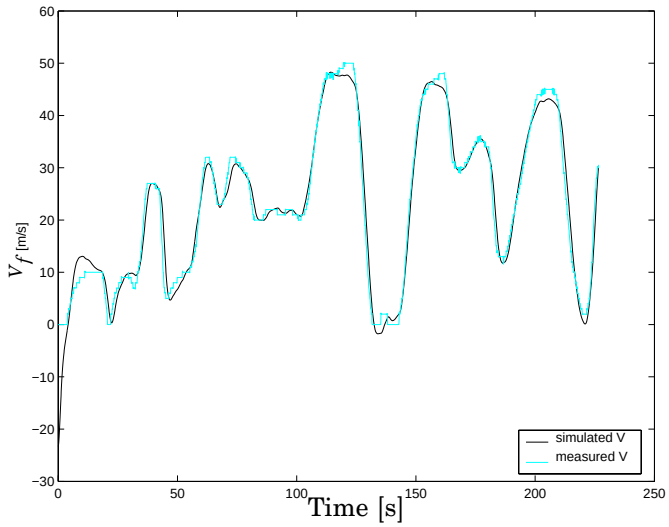

Figure 4.15 Measured velocity from the driver used in the model estimation (*dotted*) and velocity from the Simulink simulation of the model (*solid*).

measured velocity of the driver used in the estimation of the model. The models have some problem in the stop situations resulting in that the simulated vehicle reversed direction. This problem could be solve by including a saturation in the Simulink model of the brake pressure and throttle angle, a better solution would be to use the transposed brake pressure and throttle angle.

Cut-in situation

In Figs. 4.16 and 4.17, result from a 3rd and 4th order state-space model estimated by the subspace-based method is shown. The subspace-based methods have problems when there are time delays in the system. We have previously found that system of a human driver contains time delays. There is no general methods for this problem. The time delay introduces increase negative phase contribution at higher frequencies. By introducing higher order dynamics some of the phase could be captured, but it is on the cost of physical interpretation of the identified model. The 4th order state space model gives better results than the 3rd order state space model. The VAF scores for the estimated 3rd order state space model are 95.80% (b_p) and 96.91% (α_t) and for the 4th order state space model are 96.30% (b_p) and 96.93% (α_t).

Fig. 4.18 shows the cross validation result from a 4th order state-

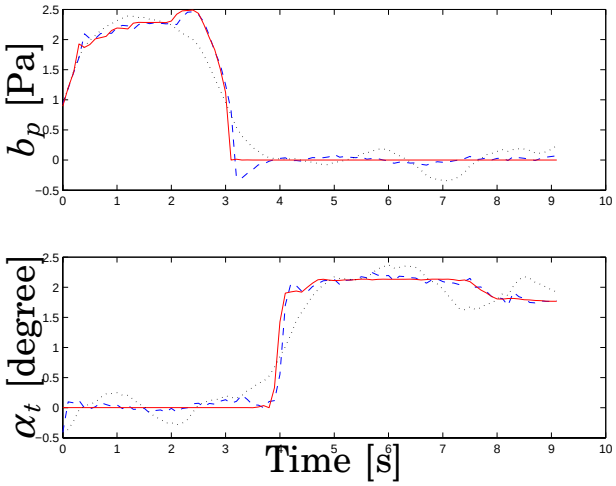

Figure 4.16 Measured b_p and α_t from a driver in a cut-in situation(*solid*). Simulated out data from a 4th order state-space model (*dotted*). Simulated out data from a 4th order one-step ahead predictor (*dashed*).

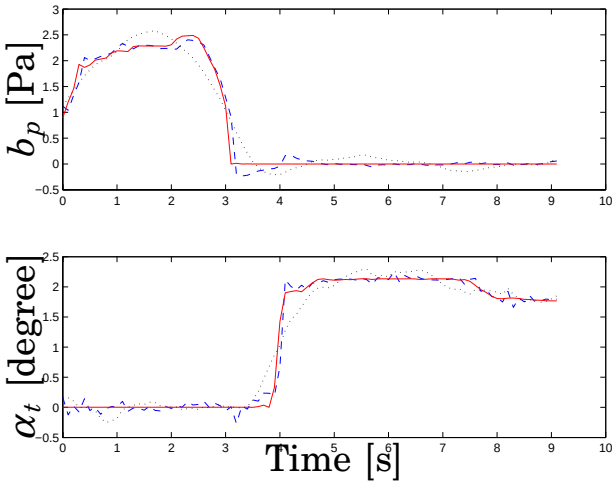

Figure 4.17 Measured b_p and α_t from a driver in a cut-in situation(*solid*). Simulated output data from a 3rd order state-space model (*dotted*). Simulated output data from a 3rd order one-step ahead predictor (*dashed*).

space model estimated by the subspace-based method, when simulating using data from another cut-in situation. The noise level is high and unknown and therefore is it not fair to compare the output of the model with the real output. As it is not possible to predict the output well on the basis of the input alone, we therefore estimated a Kalman

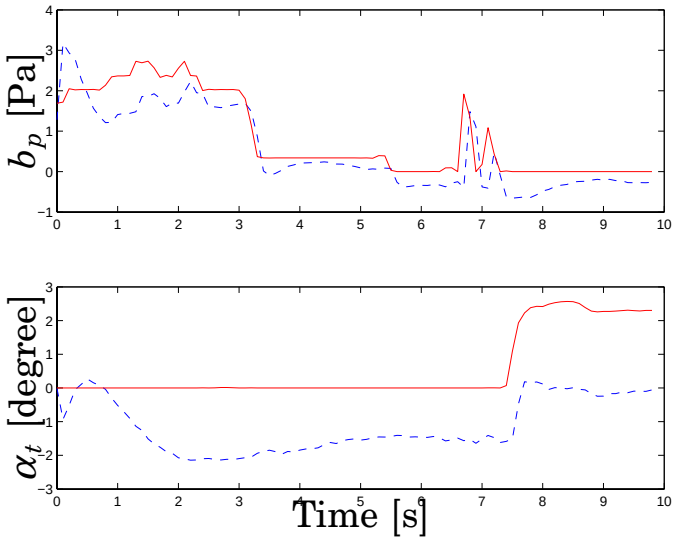

Figure 4.18 Cross validation: measured b_p and α_t from a driver in a cut-in situation(*solid*) not used in the model estimation. Simulated output data from a 4th order one-step ahead predictor (*dashed*).

filter, to build a one-step ahead predictor on the basis of our model. We noticed that the predictor have problems with low frequency gain and there is an offset between the real output and the predicted output. The VAF scores for the cross validation of the estimated 4th order one-step ahead predictor state space model are 78.33% (b_p) and 52.53% (α_t).

Brake situation

In Fig. 4.19, result from a 3rd order state-space model estimated by the subspace-based method in a braking situation is shown. The estimated low order model captures the driver behavior well by means of throttle and brake usage. The VAF scores for the estimated 3rd order state space model are 91.2% (b_p) and 92.4% (α_t).

Fig. 4.20 shows the cross validation result from a 3rd order state-space model estimated by the subspace-based method, when simulating using data from another braking situation. The model capture most of the behavior, but have problems with low frequency gain and there is an offset which lower the VAF scores. The VAF scores for the cross validation of the estimated 3rd order state space model are 91.7% (b_p) and 39.3% (α_t).

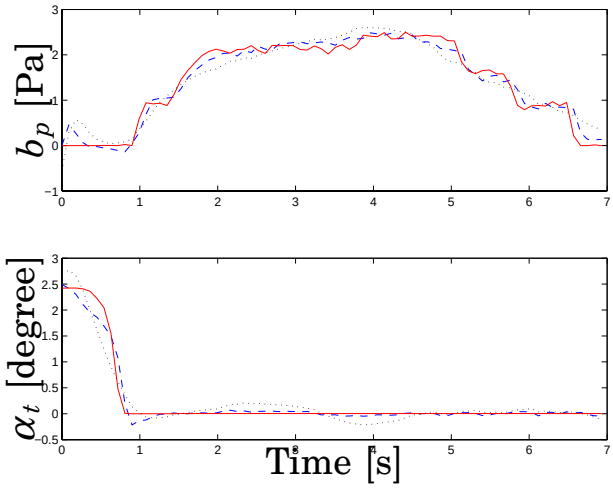

Figure 4.19 Measured b_p and α_t from a driver in a braking situation(*solid*). Simulated out data from a 3rd order state-space model (*dotted*). Simulated output data from a 3rd order one-step ahead predictor (*dashed*)

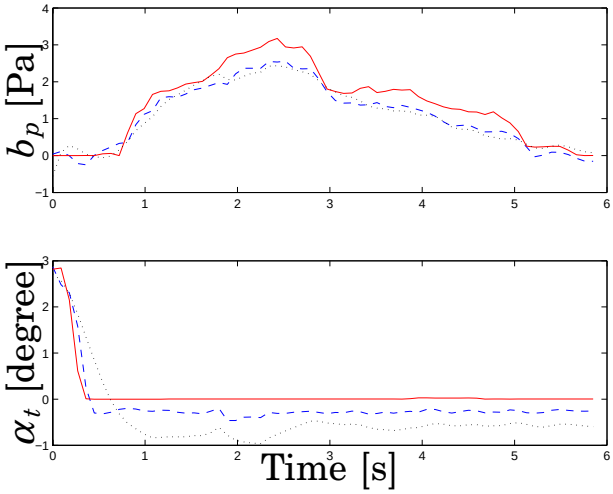

Figure 4.20 Cross validation: measured b_p and α_t from a driver in a braking situation(*solid*) not used in the model estimation. Simulated output data from a 3rd order state-space model (*dotted*). Simulated output data from a 3rd order one-step ahead predictor (*dashed*).

Approaching situation

In Fig. 4.21, result from a 3rd order state-space model estimated by the subspace-based method in a approaching situation is shown. The estimated low order model captures some of the driver behavior by

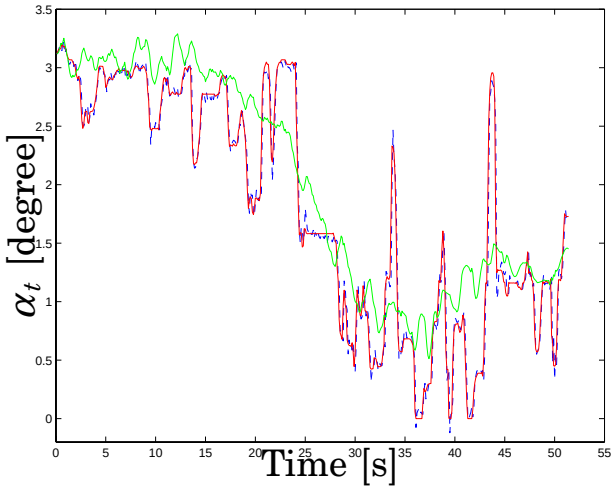

Figure 4.21 Approaching: measured α_t from one driver (*solid*) and simulated output data from a 3:rd order state-space model(*dashed*).

means of throttle usage. The VAF scores for the estimated 3rd order state space model is 80.9% (α_t).

String stability

For application in automated highway it is necessary that a stream of cars are string stable, i. e., if several vehicles are put in a row they should not give rise to oscillation causing car crashes [46]. Fig. 4.22 shows Simulink simulation result from a follow situation where 6 vehicles have been put in a row. Each vehicle is controlled by a 5th order model identified using the subspace-based method. No crash occurs in the simulation, but the oscillations grow in magnitude. Previous simulation results show that a 15th order state-space model captures the driving behavior significantly better than a 5th order state-space model and that the result can be improved using transposed signals.

4.4 Behavioral model

For the behavioral models the inputs and outputs were chosen according to system 2 (Fig. 3.5). Behavioral model of different order where estimated. The estimated model including both dynamic of the input

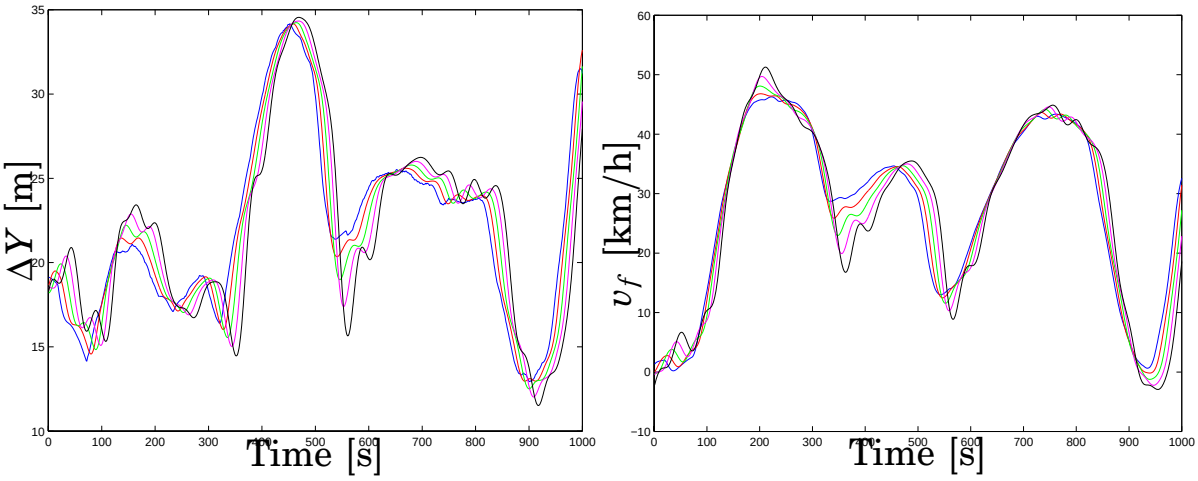

Figure 4.22 Result from a Simulink simulation with 6 vehicles in row. ΔY between the vehicles (*left*) and v_f of the vehicles (*right*).

and the outputs, since the model does not explicitly separate the signals into inputs and outputs, which is an advantage in the identification process since there are interactions between the driver and the vehicle.

Follow situation

In Fig. 4.23 a model with the total order of 30 is shown. The model fits the driver behavior well capturing both the braking behavior and the throttle behavior.

The residual analysis of the estimated 30th order model based on the behavior method is shown in Fig. 4.24. Both brake pressure and throttle angle have empirical distributions comparable with normal distributions. The VAF scores for the behavioral model are 81.9% (p_b) and 92.2% (α_t). In order to use the estimated model in an ACC-approach it is necessary to obtain from the estimated model, which contain dynamics both of the inputs and the outputs as well as the experimental condition, a input-output relation according to system 1 (Fig. 3.5). The transfer function for the input-output can be obtained by matrix fraction decomposition, but this is not a easily solved problem, since the estimated model can be divided into submodels and we want to find the subsystem which best matches the inputs and the outputs. This problem is not yet solved.

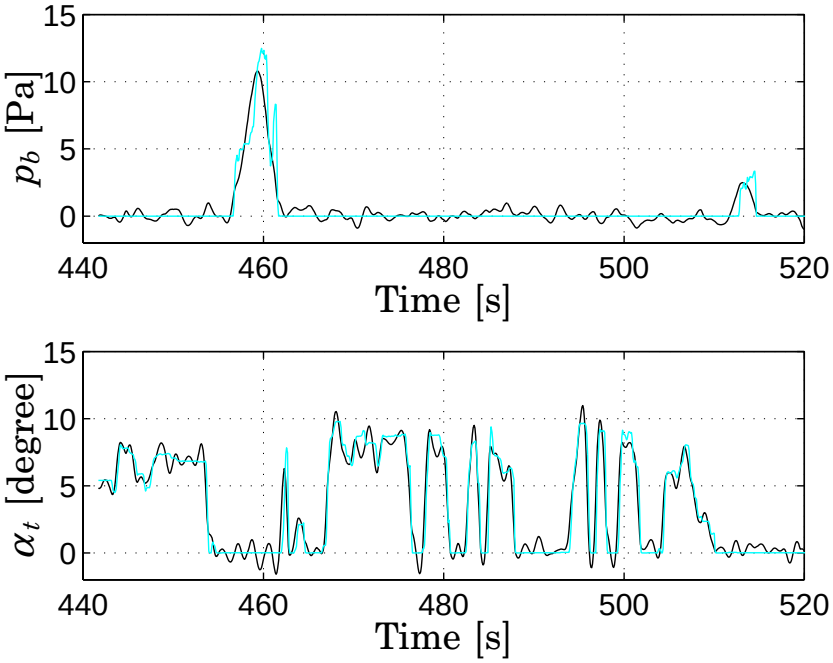

Figure 4.23 Follow: measured b_p and α_t from one driver (*grey*) and simulated output data from a behavioral model order $n = 30$ (*black*).

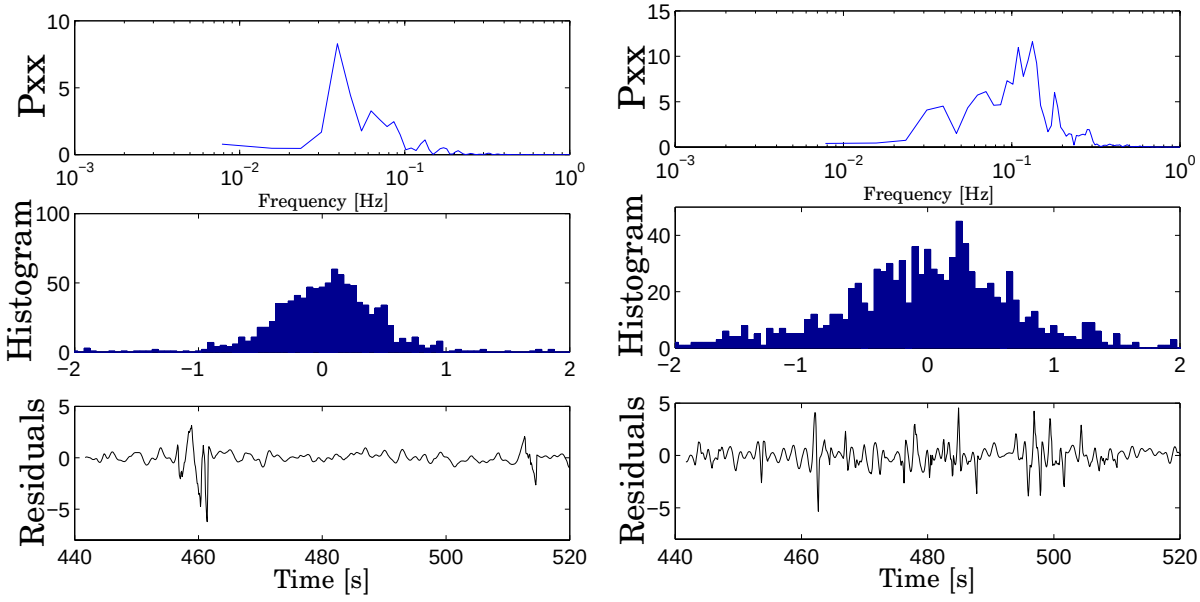

Figure 4.24 Residuals of output p_b from a behavior model $n = 30$ (*left)*. Residuals of output α_t from a behavior model $n = 30$ (*right)*. Notice that the residual of the output p_b becomes large when the time is around 460s.

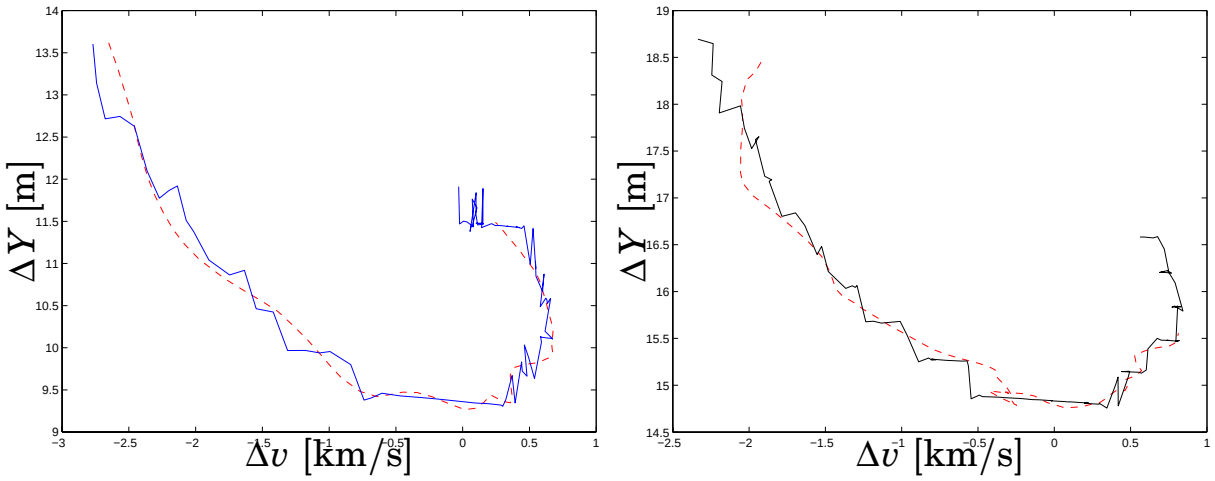

Figure 4.25 Cut-in: measured ΔY and Δv (*solid*) and simulated ΔY and Δv from a behavioral model of order $n = 10$ (*dotted*). Driver 1 (*left*) and driver 2 (*right*)

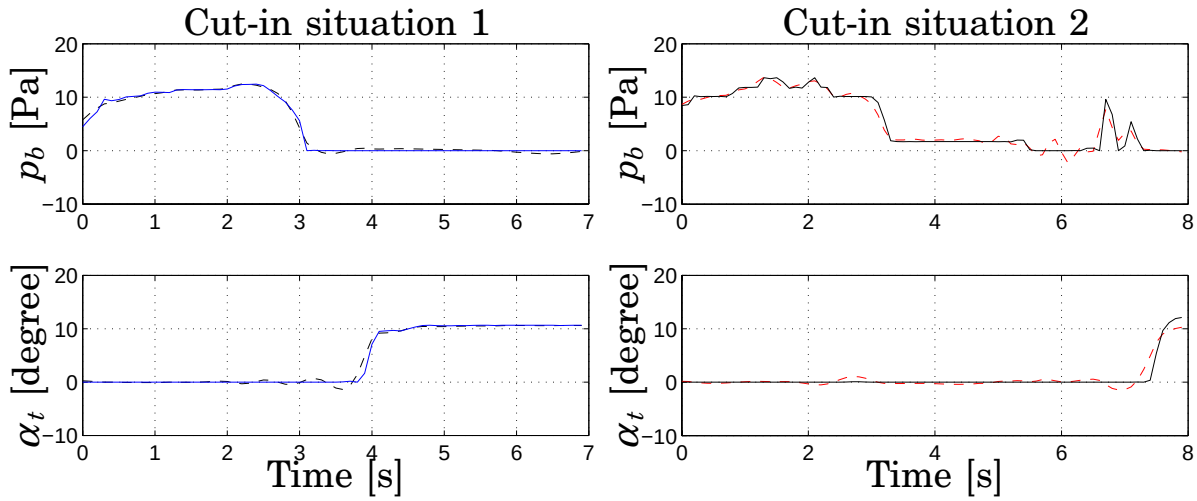

Figure 4.26 Cut-in: measured b_p and α_t from one driver (*solid*) and simulated output data from a behavioral model $n = 10$ (*dotted*).

Cut-in situation

Figs 4.25 and 4.26 show result from a estimated behavioral models of order $n = 10$ estimated from data from a cut-in situation. The model fit the measured data well, but one problem capture the driver behavior in cut-in situations is that they last only a short period of time resulting in a short data sequence. By only studying the data and the result from

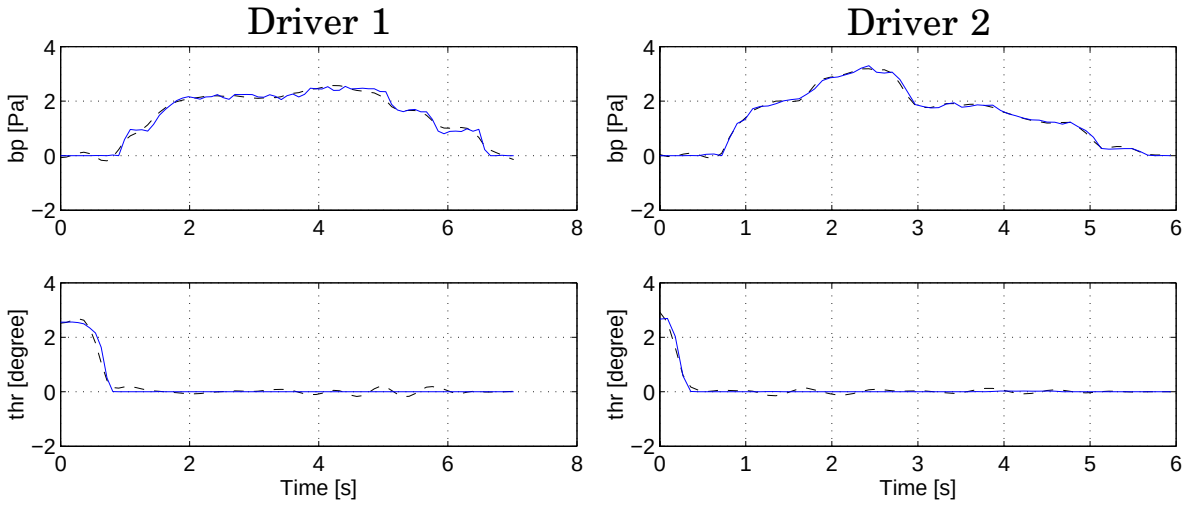

Figure 4.27 Measured b_p and α_t from one driver (*solid*) and simulated output data from a behavioral model $n = 3$ (*dotted*) from two braking situations.

the estimated model in Figs. 4.25 and 4.26 one would perhaps believe that the model could be reduced, but no good result was obtained from a behavioral model with order less than 10.

The VAF scores for the behavioral model of cut-in situation 1 are 99.3% (p_b) and 98.9% (α_t). The VAF scores for the behavior model of cut-in situation 2 are 96.1% (p_b) and 87.8% (α_t).

Brake situation

In Fig. 4.27, a result from a estimated 3rd order behavioral model in a braking situation is shown. The model captures the throttle and brake behavior well. The VAF scores for the estimated 3rd order behavioral model are 98.3% (b_p) and 97.2% (α_t).

Fig. 4.28 shows the result from the 3rd order model in the $\Delta v \Delta y$-plane and we notice that the model captures the dynamic in the braking situations.

Approaching situation

In Fig. 4.29, result from an estimated 20th order behavioral model in an approaching situation is shown. The model captures the throttle behavior well. The VAF score for the estimated 20th order behavioral model is 95.4% (α_t).

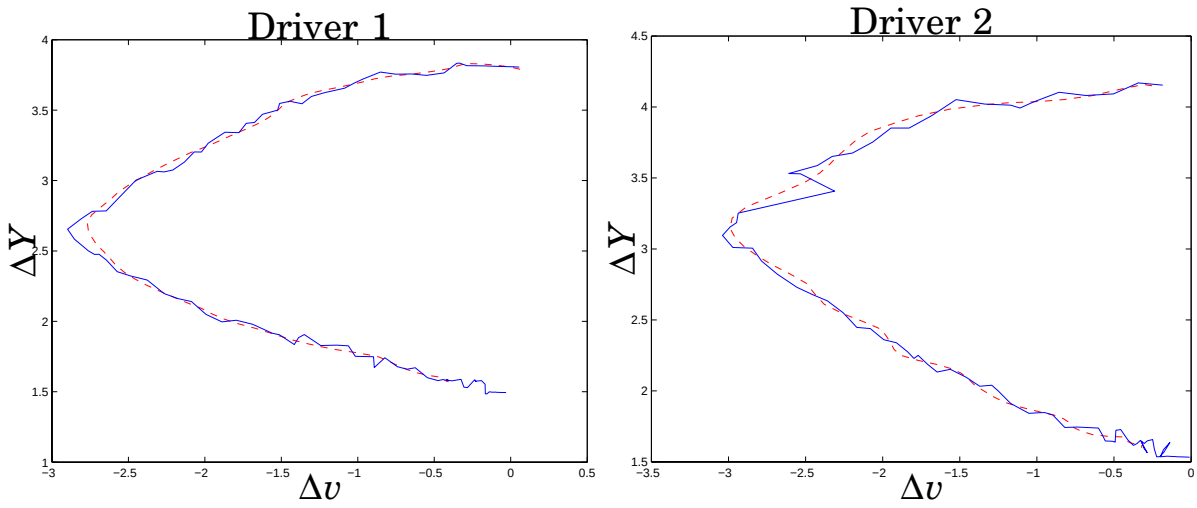

Figure 4.28 Measured $\Delta v \Delta y$-plane from two different braking situations (*solid*) and simulated $\Delta v \Delta y$-plane from a behavioral model $n = 3$ (*right*).

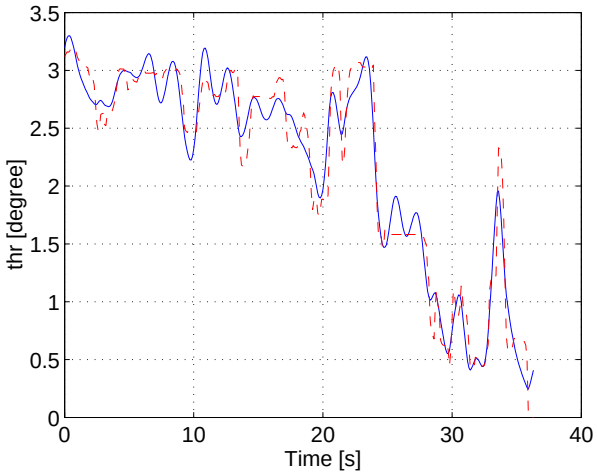

Figure 4.29 Approaching: measured α_t from one driver (*solid*) and simulated output data from a behavioral model $n = 20$ (*dashed*).

4.5 Detection and modeling of changed driver behavior

We notice that the residual ε from the 30th order behavior model for p_b becomes large when the braking starts. We may call this phenomenon 'arousal behavior' and estimate a GARCH model. In Fig. 4.30 the squared residual sequence is shown, and the residual of p_b seems to increase linearly during the brake part. The estimated third order

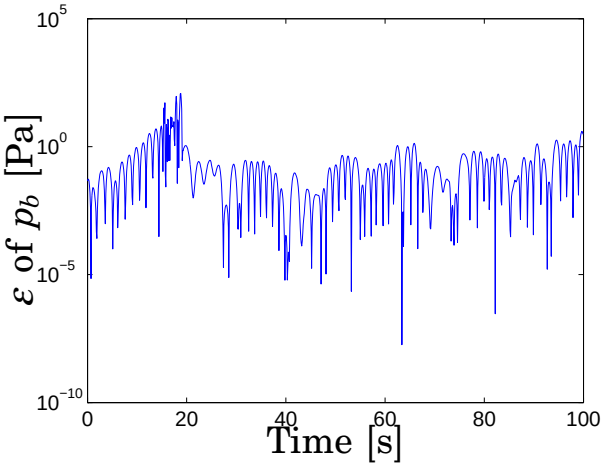

Figure 4.30 Squared residuals ε from a behavioral model of order $n = 30$. Note the change in the amplitude during the experiment.

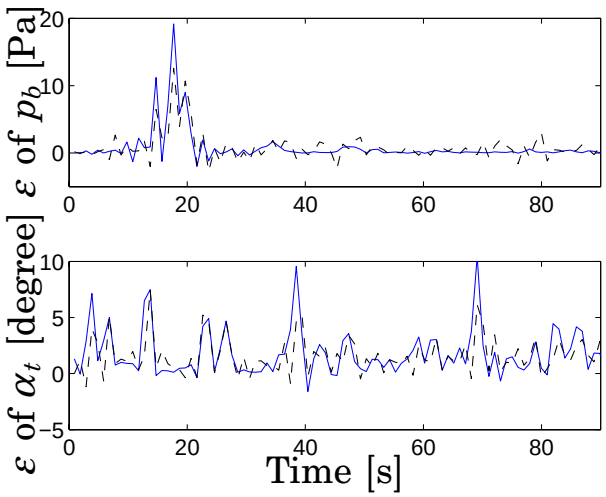

Figure 4.31 Residuals ε from driver 1 (*dashed*) and computed residuals ε from a linear regression model (*solid*).

linear regression models for the different drivers capture the behavior of the residual well, Figs. 4.31, and 4.32. A GARCH model using these amplitude varying residuals can be used for detecting when the driver changes his driving behavior. This property could be used for a hybrid model switching between different driver behavior models identified from the different traffic situations; follow, cut-in, braking and

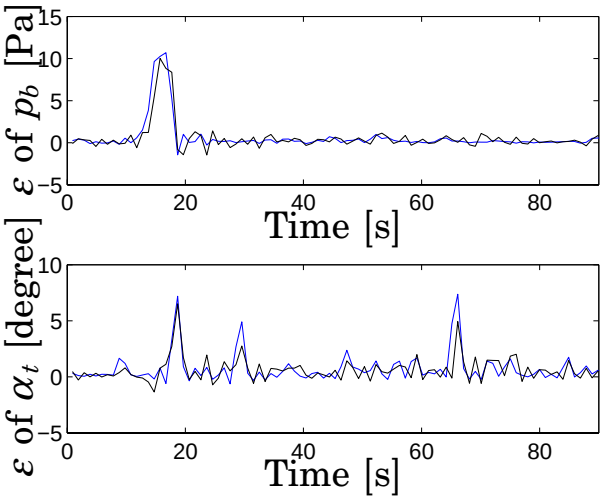

Figure 4.32 Residuals ε from driver 2 (*dashed*) and computed residuals ε from a linear regression model (*solid*).

approaching. Notice that there is an association between the arousal behavior in the brake situation and the throttle behavior, respectively.

4.6 Neural network modeling

Learning human driver behavior

Fig. 4.33 shows the results of a trained neural network when using data from one driver. The data used for training was from different follow sequences but the same driver. The trained neural network captures most of the behavior of the driver. The sequence showed is from a follow situation where the speed varies from 0 km/h to 50 km/h. Figs. 4.34 and 4.35 show results when using data which have not been used for the training (cross validation), but from the same driver and same kind of traffic situation. The result was satisfying and the neural network captures some of the behavior of the driver.

Testing of neural network model

The result from the simulation of the neural network seemed to be good, but it has to be evaluated in closed-loop situations in order to

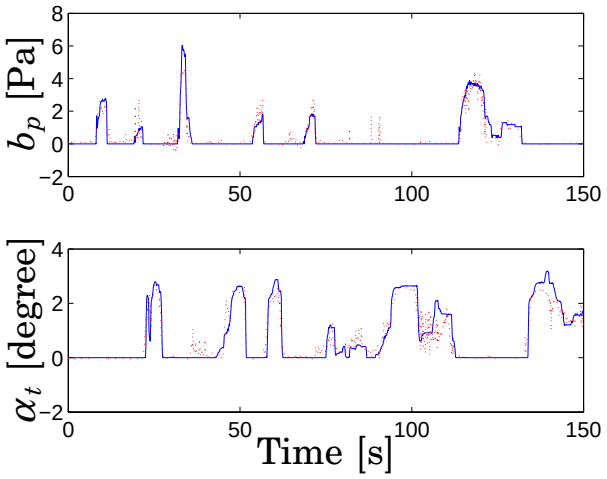

Figure 4.33 Result from the fitted neural network model. Measured b_p and α_t (*solid*) and simulated (*dotted*).

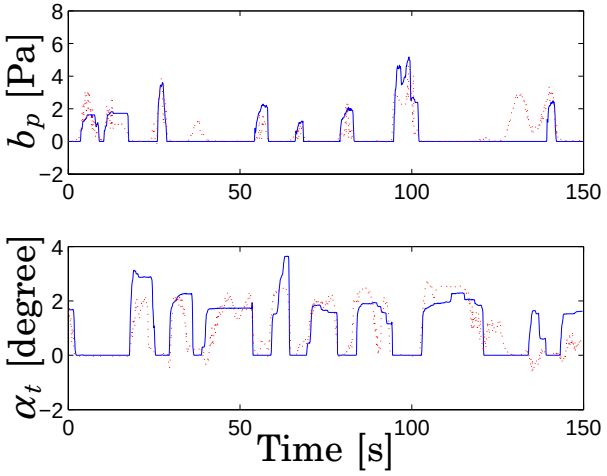

Figure 4.34 Result from the fitted neural network model, using data which was not used in the training. Measured b_p and α_t (*solid*) and simulated (*dotted*).

study their behavior. In evaluation, data from the learning was used to check the reproducing capacity. The closed-loop simulation was performed in Simulink, where the input to the system was velocity of the leader vehicle in one of the situations which was used in the training of the neural network. The results are shown in Fig. 4.36. The simulation showed that the neural network failed to reproduce the human driver

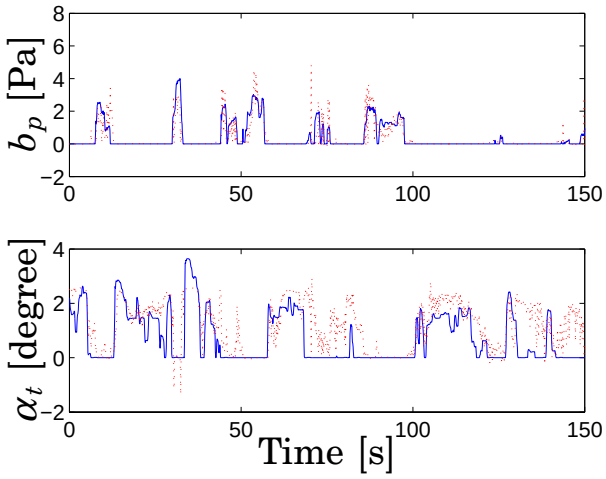

Figure 4.35 Result from the fitted neural network model, using data which was not used in the training. Measured b_p and α_t (*solid*) and simulated (*dotted*).

behavior. The problem with neural network is that you do not know how well the trained model will work in closed-loop and you have no guarantee of stability in closed-loop. This property makes the neural network difficult to use.

4.7 Summary

In this chapter we have compared results from different methods of obtaining models of human driver's longitudinal behavior; linear regression, subspace identification, behavioral model identification and neural network, with different rate of success. Best result had the behavioral model method, but there is an implementation problem in the decomposition of the behavioral model into car model and driver model. The subspace-based method gives good results, better than the ones obtained for linear regression. The neural networks showed closed-loop stability problem, which complicates their usage.

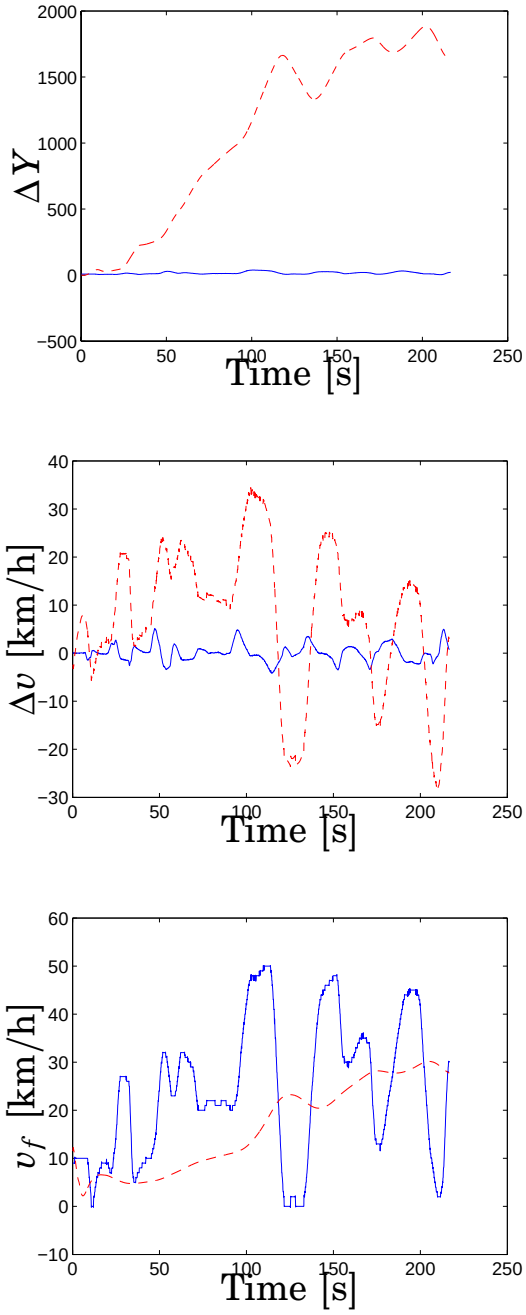

Figure 4.36 Closed-loop evaluation of the neural network model. Measured ΔY (*solid*) and simulated ΔY (*dashed*) (*upper*). Measured Δv (*solid*) and simulated Δv (*dashed*) (*middle*). Measured v_f (*solid*) and simulated v_f (*dashed*) (*lower*).

5

Discussion & Conclusions

5.1 Discussion

Human drivers use several sensors in the driving tasks: eyesight, hearing, balance organ (vestibular organ of the inner ear; vestibular nuclei), and proprioception. The central nervous system fuses the information from the sensors [31]. The vestibular system nuclei and proprioception detect changes in orientation, position and acceleration. These physological human sensors can be translated into: camera, microphone, gyro, and accelerometer. As the information rate must be manageable and since the total information rate from the sensors is huge, it is not reasonable to measure all such information.

Sensors have different significance. The eyesight (vision) is the most important sensor a human driver uses in the driving task. Thus, for practical reasons only a laser and a radar were used in the experiments.

It is known that human sensors have bandpass properties [9], which also was found in the data analysis (Figs. 3.12, 3.13). The lower limit was found around 0.1 Hz and the upper limit around 1.2 Hz. The lower limit may be explained by visual suppression, which occur in this region [39]. It has also been found that galvanic stimulation of the horizontal vestibulo-ocular reflex is not affected below 0.1 Hz [32]. In other words, there exist other physiological evidence which explain that a human driver exhibits bandpass properties. The upper limit

may be explained by the human brake reaction time, perception time and movement time, which is around 0.6-1.0s [27]. Visual suppression may also occur at high frequencies.

Seven drivers participated in the study. However, seven drivers are not enough to draw any statistical conclusions about the spread of the human driver behavior. A study with more drivers participating is needed, in order to be able to draw statistical conclusions of the driver behavior. The driver behavior of the drivers that participated in the study showed, as expected, large similarities. The major difference between the drivers consist in the choice of headway distance and aggressiveness. None of the drivers in the study were under influence of alcohol, but it would be interesting to study how this would change the driver behavior and try to model it. Such a study should be performed at a test track for safety and legal reasons.

The similarities in the driving behavior indicate that it is possible to identify a driver behavior on which most drivers would agree to be a sensible driver. A model capturing this behavior could be used in the design of an ACC system. To find a behavior which most drivers would be satisfied with is a problem which need to be studied.

Newer Volvo cars than the ones used in the experiments have a throttle controller where the acceleration is proportional to the throttle angle. This would probably improve the result of the identified models.

In retrospect extra sensor measurement like measurements of acceleration, GPS and gear information signals would have been interesting to use when studying the longitudinal driver behavior.

From the spectral analysis it was found that the drivers all had different reaction time, but it is hard to find the reaction time using spectral analysis. The experiments should have contained a part where the reaction time of the drivers was explicitly measured.

To identify physical parameters from estimated models could be interesting. This could be used for increasing understanding of driver behavior and reduction of model order.

The estimated models have only been tested in Matlab and Simulink, and an interesting next step would be to validate the model performance in real traffic situations. A related issue is how to parameterize driving comfort. One disadvantage with computer simulation is that it is hard to use in the validation of the driving comfort, as the validation has to be done in real traffic situations.

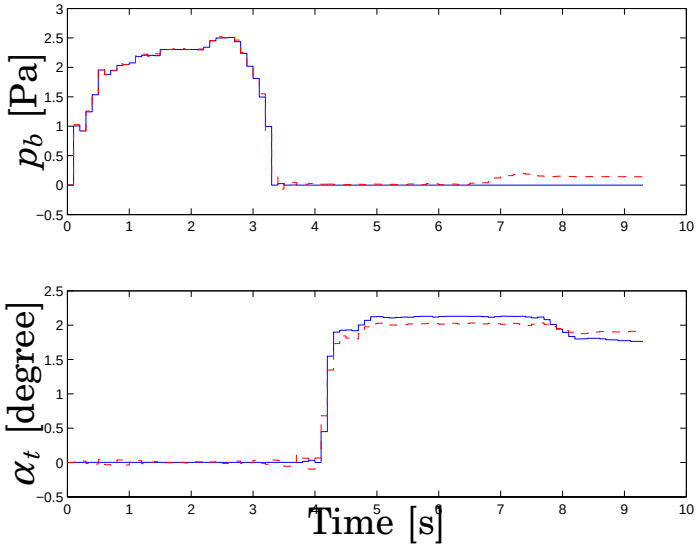

Figure 5.1 Measured b_p and α_t from one driver (*solid*) and simulated output data from a 30:th step response model (*dashed*) in a cut-in situation.

Possibly the string stability could be improved by using higher order models and transposed signals and resulting in decreased oscillations.

Normally, a cut-in situation starts with a positive step in b_p and later a step in α_t. Therefore a realization-based step-response analysis can also be used to find the dynamics of a human driver, Fig. 5.1. The method is related to realization methods for impulse-response analysis and covariance analysis and seems to work well for moderate noise levels. In Fig. 5.1 the result from a 30th order step response model is shown. To get good result a high order model had to be used, in order to capture both brake and throttle behavior.

Behavioral models are well suited for identification of driver behavior since there is no clear-cut distinction of signals as inputs and outputs. This may be preferable since there is feedback interaction between the driver and the car. The drawback is the open problem of obtaining input-output relations from the estimated model with good quality, which is needed in order to use the result in practice and for model simulation.

5.2 Conclusions

One contribution of this thesis is to describe human driver longitudinal behavior using dynamic models. Existing methods and models describing human driver behavior have been reviewed: linear and non-linear dynamic car-following models, linear optimal control models, heuristic models, neural network and fuzzy logic models, mental models, and general longitudinal models.

Another contribution is the application of existing identification methods to describe human driver's longitudinal behavior. Linear regression, subspace model identification, behavioral models and neural networks for finding dynamic models of human driver have been studied, with varying results. The result of the proposed approach using system identification was found satisfying. The models estimated have been simulated in closed-loop operation using Simulink with satisfying result. The best result was found when using the behavioral model method, but since the problem of obtaining an input-output relation for the component models in open-loop operation, the practical usefulness of the models are reduced. The estimated models using the subspace-based methods did not give as good results as the behavioral models, but still better than the linear regression models. The modeling of changes in driver behavior has been performed using GARCH models with satisfying results.

6

Bibliography

[1] P. S. Addison and D. J. Low. “A novel nonlinear car-following model.” *Chaos*, **8:4**, pp. 791–799, 1998.

[2] K. Ahmed. *Modeling Drivers’ Acceleration and Lane Changing Behavior*. PhD thesis, Massachusetts Institute of Technology, Cambridge, 1999.

[3] B. D. O. Anderson and J. B. Moore. *Optimal Control Linear Quadratic Methods*. Prentice Hall, New Jersey, 1990.

[4] G. A. Bekey and G. O. Burnham. “Control theoretic models of human drivers in car-following.” *Human Factors*, **No 19**, pp. 399–413, 1977.

[5] R. F. Benekohal and J. Treiterer. “Carsim: Car-following model for simulation of traffic in normal and stop-and-go conditions.” *Transportation Research Record 1194*, pp. pp. 99–111, 1998.

[6] T. Bleile. “A new microscopic model for car-following behavior in urban traffic.” In *Proceedings 4th World Congress on Intelligent Transport Systems*, Berlin, 1997.

[7] E. R. Boer and M. Hoedemaeker. “Modeling driver behavior with different degrees of automation: A hierarchical decision framework of interacting mental models.” In *Proceedings of the XVIIth European Conference on Human Decision Making and Manual Control*, Valenciennes, 1998.

[8] T. Bollerslev. “Generalized autoregressive conditional heteroskedasticity.” *J. of Econometrics*, **31**, pp. 307–327, 1986.

[9] T. Brandt. *Vertigo : Its Multisensory Syndromes*. Springer, Berlin, 2:nd edition, 1999.

[10] R. E. Chandler, R., Herman, and E. Montroll. "Traffic dynamics: studies in car following." *Operation Research*, **No 6**, 1958.

[11] L. C. Edie, R. S. Foote, R. Herman, and R. Rorthery. "Analysis of single lane traffic flow." *Traffic Engineering 2*, **33**, pp. 21–27, 1963.

[12] D. C. Gazis, R. Herman, and B. Potts. "Car-following theory of steady-state traffic flow." *Operation Research*, **No 9**, 1959.

[13] D. C. Gazis, R. Herman, and R. W. Rothery. "Nonlinear follow-the-leader models of traffic flow." *Operation Research*, **No 9**, 1961.

[14] S. Germann and R. Isermann. "Nonlinear distance and cruise control for passenger cars." In *Proceedings of the American Control Conference*, vol. 1, pp. 3081–3085, 1995.

[15] A. Ghazi Zadeh, A. Fahim, and M. El-Gindy. "Neural network and fuzzy logic applications to vehicle systems: literature survey." *Journal of Vehicle Design*, **18:2**, 1997.

[16] P. G. Gipps. "A behavioural car-following model for computer simulation." *Transport Research-B*, **15**, pp. 105–111, 1981.

[17] M. A. Goodrich and E. R. Boer. "Semiotics and mental models: Modeling automobile driver behavior." In *Proceeding of the 1998 IEEE ISIC/ CIRA/ ISAS Joint Conference*, pp. 771–776, Gaithersburg, 1998.

[18] R. Gray and D. Regan. "Accuracy of estimating time to collision using binocular and monocular information." *Vision Research*, pp. 499–512, 1998.

[19] N. C. Griswold, N. D. Kehtarnavaz, and K. M. Miller. "A transportable neural network controller for autonomous vehicle following." In *Intelligent Vehicles '94 Symposium*, pp. 195–200. 1994.

[20] M. T. Hagan and M. Menhaj. "Training feedforward networks with the Marquardt algorithm." *IEEE Transactions on Neural Networks*, **5:6**, pp. 989–993, 1994.

[21] J. D. Hamilton. *Time Series Analysis*. Princeton University Press, Princeton, NJ, 1994.

[22] B. Haverkamp. *Subspace Model Identification, theory and practice.* PhD thesis, Delft University of Technology, Netherlands, Delft, 2000.

[23] J. Hitz, J. Koziol, and A. Lam. "Safety evaluation results from the field operational test of an intelligent cruise control (ICC) system." Number 2000-011352 in SAE Technical Paper Series, 2000.

[24] T. Iijima, A. Higashimata, S. Tange, K. Mizoguchiand, H. Kamiyama, K. Iwasaki, and K. Egawa. "Development of an adaptive cruise control system with brake actuation." Number 2000-01-1353 in SAE Technical Paper Series, 2000.

[25] P. A. Ioannou and C. C. Chen. "Autonomous intelligent cruise control." *IEEE Transactions on Vehicular Technology*, **42:4**, 1993.

[26] J.-S. R. Jang, C.-T. Sun, and E. Mizutani. *Neuro-Fuzzy and Soft Computing*. Prentice Hall, New Jersey, 1997.

[27] G. Johansson and K. Rumar. "Driver brake reaction times." *Human Factors*, **No 13**, pp. 23–27, 1972.

[28] R. Johansson. *System Modeling and Identification*. Prentice Hall, Englewood Cliffs, NJ, 1993.

[29] R. Johansson, M. Verhaegen, C. T. Chou, and A. Robertsson. "Behavioral model identification." In *IEEE Conf. Decision and Control (CDC'98)*, pp. 126–131, Tampa, Florida, December 1998.

[30] P. N. Johnson-Laird. *The Computer and the Mind: An Introduction to Cognitive Science*. Harvard University Press, Cambridge, 1998.

[31] E. R. Kandel, J. H. Schwartz, and T. M. Jessell. *Principles of Neural Science (4th ed).* McGraw-Hill, New York, 2000.

[32] M. Karlberg, L. McGarvie, M. Magnusson, S. Aw, and G. Halmagyi. "The effects of galvanic stimulation on the human vestibulo-ocular reflex." *Neuroreport*, **11:17**, pp. 3897–3901, 2000.

[33] U. Kiencke and L. Nielsen. *Automotive Control Systems For Engine, Driveline, and Vehicle*. Springer, Berlin, 2000.

[34] N. Kuge, T. Yamamura, O. Shimoyama, and A. Liu. "A driver behavior recognition method based on a driver model framework." Number 2000-01-0349 in SAE Technical Paper Series, 2000.

[35] D. N. Lee. "A theory of visual control braking based on information about time-to-collision." *Perception*, **5**, pp. 437–459, 1976.

[36] W. Leutzbach. *Introduction to the Theory of Traffic Flow*. Springer-Verlag, Berlin, 1988.

[37] J. Ludmann and D. Neunzig. "The effectivity of new traffic technologies in suburban areas - an analysis with the microscopic traffic simulator PELOPS." In *AVEC '96, International Symposium on Advanced Vehicle Control*. 1401-1432, 1996.

[38] A. May and H. Keller. "Non-integer car-following models." *Highway research Record 199*, p. 32, 1967.

[39] J. Meiry. *Vestibular and proprioceptive stabilization of eye moments*. In The control of eye movements. Academic Press, New York, 1971.

[40] O. Nakayama, T. Futami, T. Nakamura, and E. R. Boer. "Development of a steering entropy method for evaluating driver workload." Number 1999-01-0892 in SAE Technical Paper Series, 1999.

[41] M. Persson, F. Botling, E. Hesslow, and R. Johansson. "Stop and go controller for adaptive cruise control." In *Proceedings of the 1999 IEEE international Conference on Control Applications*, vol. 2, pp. 1692–1697, 1999.

[42] L. A. Pipes. "An operational analysis of traffic dynamics." *Journal of Applied Physics*, **24**, pp. 271–281, 1953.

[43] W. Prestl, T. Sauer, J. Steinle, and O. Tschernoster. "The BMW active cruise control ACC." Number 2000-01-0344 in SAE Technical Paper Series, 2000.

[44] J. Rasmussen. *Outlines of a hybrid model of the process plant operator*. Plenum, 1976.

[45] H. Subramanian. “Estimation of car-following models.”. Master’s thesis, MIT, Department of Civil and Environmental Engineering, 1996.

[46] D. Swaroop. *String Stability of Interconnected Systems: An Application to Platooning in Automated Higway Systems*. PhD thesis, University of California, Berkeley, Berkeley, 1997.

[47] C. Thorpe, T. Joechem, and D. Pomerleau. “The 1997 automated highway free agent demonstration.” In *Intelligent Transportation System, ITC ’97*, pp. 496–501, 1997.

[48] A. R. A. van der Horst. *A time-based analysis of road user behaviour in normal and critical encounters*. PhD thesis, Institute for Perception TNO, 1990.

[49] W. van Winsum and A. Heino. “Choice of time-headway in car-following and the role of time-to-collision information in braking.” *Ergonomics*, **No 4**, pp. 579–592, 1996.

[50] M. Verhaegen and P. Dewilde. “Subspace model identification—analysis of the elementary output-error state-space model identification algorithm.” *Int. J. Control*, **56**, pp. 1211–1241, 1992.

[51] M. Verhaegen and P. Dewilde. “Subspace model identification—the output-error state-space model identification class of algorithms.” *Int. J. Control*, **56**, pp. 1187–1210, 1992.

[52] G. Widmann, M. Daniels, L. Hamilton, L. Humm, B. Riley, J. Schiffmann, D. Schnelker, and W. Wishon. “Comparison of lidar-based and radar-based adaptive cruise control systems.” Number 2000-01-0345 in SAE Technical paper Series, 2000.

[53] R. Wiedermann. *Simulation des Strassenverkehrsflusses*. Schriftenreihe des Institutes für Verkehrswesen der Universität Karlsruhe, 1974.

[54] J. C. Willems. “From time series to linear systems. Part I: Finite dimensional linear time invariant systems, and Part II: Exact modeling.” *Automatica*, **22**, pp. 561–80 and 675–694, 1986.

[55] Q. Yang and H. N. Koutsopoulos. “A microscopic traffic simulator for evaluation of dynamic traffic management systems.” *Transportation Research C*, **4**, pp. 113–129, 1996.